EUROFUSION WPJET1-PR(16) 16628

F Koechl et al.

Modelling of Transitions Between L- and H-Mode Including Tungsten Behaviour in JET and ITER Scenarios

Preprint of Paper to be submitted for publication in
Nuclear Fusion

This work has been carried out within the framework of the EUROfusion Consortium and has received funding from the Euratom research and training programme 2014-2018 under grant agreement No 633053. The views and opinions expressed herein do not necessarily reflect those of the European Commission.

Modelling of Transitions Between L- and H-Mode Including Tungsten Behaviour in JET and ITER Scenarios

F Koechl[1], A Loarte[2], V Parail[3], P Belo[3], M Brix[3], G Corrigan[3], D Harting[3], T Koskela[4,5], A S Kukushkin[2,*], A R Polevoi[2], M Romanelli[3], G Saibene[6], R Sartori[6], T Eich[7] and JET Contributors[**]

EUROfusion Consortium, JET, Culham Science Centre, Abingdon, OX14 3DB, UK

[1]TU Wien, Atominstitut, 1020 Vienna, Austria
[2]ITER Organization, Route de Vinon-sur-Verdon - CS 90 046 - 13067 St Paul Lez Durance Cedex, France
[3]CCFE, Culham Science Centre, Abingdon, OX14 3DB, UK
[4]Aalto University School of Science, P.O.Box 15100, 00076 AALTO, Finland
[5]NERSC, Lawrence Berkeley National Laboratory, 1 Cyclotron Road, Berkeley, CA, 94720
[6]Fusion For Energy Joint Undertaking, Josep Pla 2, 08019, Barcelona, Spain
[7]Max Planck Institute for Plasma Physics, 85748 Garching, Germany
e-mail address: Florian.Koechl@ukaea.uk

Abstract

The dynamics for the transition from L-mode to a stationary high Q_{DT} H-mode regime in ITER is expected to be qualitatively different to present experiment due to low fuelling efficiency of recycling neutrals, that influence the post transition plasma density evolution, and the effect of the plasma density evolution itself both on the alpha heating power and the edge power flow required to sustain the H-mode confinement itself. This paper presents results of modelling studies of the transition to stationary high Q_{DT} H-mode regime in ITER with the JINTRAC suite of codes, which include optimisation of the plasma density evolution to ensure a robust achievement of high Q_{DT} regimes in ITER on the one hand and the avoidance of tungsten accumulation in this transient phase on the other hand.

As a first step, the JINTRAC integrated models have been validated against core, pedestal and divertor plasma measurements in JET experiments for the transition from L-mode to stationary H-mode in ITER relevant conditions (highest achievable current and power, $H_{98,y} \sim 1.0$, low collisionality, comparable evolution in P_{net}/P_{L-H}). Good agreement between code predictions and measured plasma parameters is obtained if anomalous transport in the edge transport barrier is reduced with increasing edge power flow normalised to the H-mode threshold; in particular the increase in edge plasma density is dominated by this edge transport reduction as the calculated neutral influx across the separatrix remains unchanged (or even slightly decreases) following the H-mode transition.

JINTRAC modelling of H-mode transitions for the ITER 15 MA / 5.3 T high Q_{DT} scenarios with the same modelling assumptions as those being derived from JET experiments has been carried out. The modelling

---

[*] Present addresses:
NRC Kurchatov Institute, Kurchatov sq. 1, 123182 Moscow, Russia
NRNU MEPhI, Kashirskoje av. 31, 115409 Moscow, Russia

[**] See the author list of "Overview of the JET results in support to ITER" by X. Litaudon et al. to be published in Nuclear Fusion Special issue: overview and summary reports from the 26th Fusion Energy Conference (Kyoto, Japan, 17-22 October 2016)

finds that it is possible to access high Q_{DT} conditions robustly for additional heating power levels of $P_{AUX} \geq 53$ MW by optimising core and edge plasma fuelling in the transition from L-mode to high Q_{DT} H-mode. An initial period of low plasma density, in which the plasma accesses the H-mode regime and the alpha heating power increases, needs to be considered after the start of the additional heating, which is then followed by a slow density ramp. Both the duration of low density phase and the density ramp-rate depend on boundary and operational conditions and can be optimised to minimise the resistive flux consumption in this transition phase. The modelling also shows that fuelling schemes optimised for a robust access to high Q_{DT} H-mode in ITER are also optimum for the prevention of the contamination of the core plasma by tungsten during this phase.

1. Introduction

The dynamics of the access to high Q_{DT} plasmas in the H-mode confinement regime in ITER is expected to be qualitatively different from that of present experiments because:
a) fuelling by cold neutrals is expected to be much less effective in ITER than in present experiments [Romanelli NF 2015] yielding a different edge density evolution after the transition from L-mode to H-mode,
b) the ITER heating methods (ECRH, ICRH and high energy (1 MeV) NBI), do not lead to significant core fuelling [Loarte NF 2013],
c) the ratio between the heat flux crossing the separatrix and the L-H transition threshold power is moderate ($P_{sep}/P_{L-H} < 2.0$ even in stationary $Q_{DT} \sim 10$ burning conditions) [Hawryluk NF 2009],
d) the evolution of the plasma density in ITER not only determines the power required to access the H-mode regime but also influences the evolution of the alpha heating power which in turn affects the rate of the change in plasma energy after the transition [Kessel NF 2015],
e) in addition to the difference in these physics phenomena in ITER, operation with a W divertor may impose additional operational constraints due to possible W accumulation and increased core plasma radiation in the transient H-mode access phase which could lead to a decrease of the edge power flow and a return to L-mode confinement.
Simple extrapolation from present experiments to ITER relying on empiric scaling laws for the description of ITER H-mode access characteristics may be inappropriate, as these differences would not be considered. However, they can be taken into account in an integrated time-dependent transport modelling approach.

In order to determine, under which conditions the transition to stationary high Q_{DT} H-modes can be achieved in ITER and how the plasma evolution to H-mode can be optimised in this phase, and to assess the issues related to edge and core W transport in this phase, integrated ITER core+edge and core+edge+SOL modelling studies have been performed with the JINTRAC suite of codes [Romanelli PFR 2014] with the abovementioned ITER specific characteristics being implicitly taken into account. This paper describes these studies and their main conclusions.

Since the core, edge transport barrier (ETB) and SOL transport model assumptions that are applied in JINTRAC to predict the plasma behaviour in ITER in the transition to high Q_{DT} H-mode have only partly been validated against measurements for the L-H transition in existing tokamaks so far [Militello-Asp EPS 2013], fully integrated core+edge+SOL simulations have

first been carried out for a set of selected JET plasma discharges. These discharges have plasma conditions as close as possible to those expected in ITER in terms of plasma current, auxiliary power, quality of the confinement, density in relation to the Greenwald density, collisionality, and the evolution in P_{net}/P_{L-H} after the L-H transition and correspond to operation with carbon plasma facing components at JET [Nunes NF 2013]. Detailed comparison of JINTRAC modelling predictions for these discharges can thus be used to identify the transport models that describe best the plasma behaviour in this phase including the change of the level of edge anomalous transport from that typical of L-mode plasmas to high confinement H-modes during this phase. The effects of the changes in the models and modelling assumptions for the core, ETB and SOL on the modelled plasma parameters in these three regions, can be compared with the experimental data to identify the transport models and modelling assumptions that best describe the JET ITER-like plasmas.

The JINTRAC transport core, ETB and SOL transport models and assumptions validated against JET experiments can then be applied to simulate the transition phase from L-mode to stationary high quality H-mode in the ITER 15 MA / 5.3 T high Q_{DT}. As mentioned above, there are significant differences between plasma behaviour in this transition in ITER compared to present experiments. Modelling this transition phase with validated models and assumptions allows the quantitative identification of the processes that will be at play in ITER as well as the use of externally controlled actuators (additional heating and core and edge fuelling) to optimise plasma behaviour in this phase. Of particular concern are the build-up of the alpha heating power that eventually dominates the stationary phase of high Q_{DT} H-modes in ITER as well as the control of W contamination of the core plasma during this phase which can cause large radiative losses and, if excessive, prevent the plasma from accessing the high confinement H-mode phase.

This paper is structured as follows. Section 2 describes the models and the main modelling assumptions applied to the L-mode and H-mode plasmas and to the transition between these two confinement regimes. Section 3 describes the comparison of the modelling predictions with SOL, pedestal and core plasma measurements in the H-mode access phase of ITER-like plasmas at JET and the choice of modelling assumptions that reproduced best the experimental data. Section 4 describes the results of modelling the H-mode access phase of ITER 15MA/5.3T high Q_{DT} scenarios with the JET-validated assumptions, identifies the conditions required for the robust access to high Q_{DT} burning H-mode and explores the operational possibilities to optimise this high performance H-mode access phase. Section 5 deals with the specific aspects related to W transport and core contamination during the H-mode transition phase and Section 6 summarizes the conclusions of our studies.

2. Set-up of simulations, main transport models and modelling assumptions

The JINTRAC simulations described in this paper are fully predictive simulations in which the equations of current diffusion, main ion and impurity particle and electron and ion heat transport are solved. Simulations have been performed both with the 1.5D core+edge transport codes JETTO+SANCO (JINTRAC-Core), using effective boundary conditions derived from SOL

transport models for the confined region, and with the complete set of JINTRAC transport codes for the full plasma volume including the core, edge and the SOL, i.e. JETTO+SANCO coupled to EDGE2D+EIRENE, (JINTRAC-Core+SOL).

Core plasma transport in the L-mode phase is modelled with the standard Bohm/gyroBohm (BgB) model [Erba JET Report 1996] considering an inward pinch proportional to $D_{BgB,main\ ion}$ [Coppi NF 1981, 4, Behringer IAEA 1981]. For H-mode conditions, the GLF23 transport model [Waltz PoP 1997] or a retuned version of BgB fitted to GLF23 predictions in ITER baseline high current plasmas [Garzotti NF 2012, Romanelli NF 2015] (with inward particle pinch) is used for the plasma core transport. The plasma confinement mode (L-mode or H-mode) is determined by comparing the power required to access the H-mode (P_{L-H}) evaluated with the scaling from [Martin JPhys 2008] with the net heat flux $P_{net} = P_{tot} - dW_{th}/dt$ (neglecting core radiation as it is also not considered in the derivation of the scaling for P_{L-H}). With BgB, anomalous impurity particle diffusivities and pinch velocities are taken to be identical with those for main ions, whereas with GLF23, impurity-specific D_{imp} and v_{imp} are calculated (using local averages for the impurity charge and mass numbers). Neoclassical transport in the core and ETB is predicted by NCLASS [Houlberg PoP 1997] for main ions and all impurity stages except for W transport, which is described by application of a bundling scheme with six super-stages in SANCO [Summers AIP 2007].

Following the H-mode transition, the level of anomalous energy and particle transport in the ETB is decreased by the application of a suppression factor $\exp(-(P_{net}-P_{L-H})/(\lambda_{\chi/D}\cdot P_{L-H}))$ that mimics the gradual improvement in H-mode confinement as P_{net} becomes larger than P_{L-H}, which is observed in the experiment. When $P_{net} >> P_{L-H}$ the energy and particle transport in the ETB reaches the levels of neoclassical transport. The value of the constants λ_χ, λ_D that determine the rate of the reduction of the energy and particle diffusivities χ and D with increasing P_{net}/P_{L-H} are adjustable in the model and have been inferred from the comparison of model predictions against measurements of plasmas undergoing L-H transitions, as described for ITER-like plasmas in the next section.

ELM-induced transport in the ETB is modelled in a time averaged way with the continuous ELM model [Parail NF 2009], where a maximum normalised pressure gradient in the ETB is imposed that yields a pedestal pressure close to EPED1 predictions [Snyder PoP 2009, Polevoi NF 2015]. The ETB width has either been prescribed and matched with EPED1 predictions or it has been directly determined by the EPED1 scaling in the simulation. Resistivity and bootstrap current density are calculated by NCLASS.

Auxiliary heating by neutral beams is modelled with the PENCIL [Challis NF 1989] or ASCOT [Heikkinen PoP 1995] codes. ICRH heating is modelled with the PION [Eriksson NF 1993] code, and ECRH is modelled with a scaling approximation based on GRAY calculations [Farina FSciTec 2007].

Fuelling of the confined plasma (core +ETB) is realised by high energy neutrals from the neutral beams (negligible in ITER), neutral atoms originated from gas puffing and plasma recycling (a small contribution in ITER and more significant in JET) and by pellets (in the ITER DT plasmas modelled).

Pellet fuelling is described either by a continuous pellet source with a peak in particle deposition at $\rho_{norm} \sim 0.85$ (corresponding to typical pellet code predictions for high field side pellet injection considering the ExB drift of the ionised ablated pellet particle cloudlets in ITER H-mode target plasmas [Pégourié PPCF 2009]) or by the pellet code HPI2 [Pégourié NF 2007]. The amplitude of the source profile (for the continuous pellet model) or the frequency of pellet injection (for a chosen pellet size) is adjusted in the code by feedback control on a prescribed target for the evolution of the ITER plasma average electron density.

The magnetic equilibrium is updated every ~100 ms with the 2D equilibrium solver ESCO (considering the pressure contribution from fast particles).

In integrated core+edge+SOL simulations, standard ITER or JET wall and pump structures and assumptions are applied [Romanelli NF 2015, Romanelli PFR 2014, Groth JNM 2015]. The standard Braginskij model is used for the parallel heat and particle transport in the SOL [Braginski RevPP 1965]. Perpendicular transport in the near-SOL is assumed to be equal to its 1-D counterpart at the separatrix for both L-mode and H-mode plasma conditions. Further away from the separatrix (at $R\text{-}R_{sep} > \sim 0.5$ cm in the outer midplane) the heat and particle diffusivities gradually approach a constant level with typical values of $\chi_e = \chi_i = 1.0\ m^2/s$, $D_{D/T} = D_{imp} = 0.3\ m^2/s$. This assumption about perpendicular transport allows the anomalous transport in the near-SOL (both for heat and particle fluxes) to drop to a very low level after the L-H transition as the near-SOL transport reflects the strong reduction of the edge transport in the ETB following the H-mode transition, which is in agreement with experimental observations [Neuhauser EPS 1999]. Drifts in the SOL are not included in the simulations.

The maximum time step used for the integration of the transport equations in EDGE2D is 10^{-5} s. For the description of neutral dynamics, 20000 Monte Carlo particles have been used in EIRENE at each iteration. Regarding other edge modelling assumptions, the standard EDGE2D+EIRENE plasma-wall interaction models are used. The same set of impurities is considered in EDGE2D+EIRENE as with JINTRAC-Core. In the simulations for ITER including here the effect of prompt W re-deposition is not taken explicitly into account.

Special modelling assumptions that apply to a specific limited set of simulations only are described in the next sections when these simulations are discussed.

3. L-H transition in ITER-relevant JET plasmas with Carbon Plasma Facing Components

Integrated JINTRAC-Core+SOL simulations have been carried out in order to validate transport assumptions for the modelling of the L-H transition and the access to stationary high quality H-

mode in ITER with JET plasmas. The phase from L-mode to stationary H-mode of two JET high current discharges #79668 and #79688 with plasma current I_p = 3.5-3.8 MA, NBI heating power level P_{NB} ~ 19-21 MW and high quality H-mode energy confinement with plasma energy W_{th} ~ 8-10 MJ, with Carbon Plasma Facing Components (PFCs) have been considered for detailed modelling. These plasma conditions have been chosen as they have been identified to be representative for ITER regarding core and pedestal plasma due to the low core fuelling by the JET NBI injectors in these plasma conditions and the low core and pedestal H-mode plasma collisionalities achieved [Loarte NF 2013]. These conditions have not been reproduced so far with tungsten and beryllium PFC operation in JET (so called ITER-like Wall PFCs or ILW). The specific discharges subject to detailed comparison with modelling have been selected because of the availability of high quality measurements for the plasma in the core, the edge transport barrier and (for one of them, cf. subsection 3.1) of divertor target power fluxes.

In the core region, transport equations are solved with high resolution (300 mesh points) for current diffusion, electron and ion heat, D main ions and C impurities, while toroidal velocity is prescribed using measurements from charge-exchange spectroscopy. In the SOL, the parallel momentum equations are solved, but currents are neglected. Anomalous core transport is modelled with GLF23, neoclassical core and ETB transport is modelled by NCLASS. Sawteeth have not been included in the simulations, as they are almost absent in the experiment in the transition phase from L-mode to H-mode (cf. core temperature evolution in Figs. 4 and 18), which is of most interest, and only become relevant when stationary ELMy H-mode conditions are reached. Neglecting the sawteeth leads to a slight overestimation of the stationary H-mode core plasma temperatures and densities modelled as the effective transport level does not include their effect.

The plasma equilibrium and SOL magnetic geometry is determined by the EFIT code. Inside the EFIT separatrix, the magnetic equilibrium is recalculated every ~90 ms by the 2-D equilibrium solver ESCO with high resolution (300x300 mesh points), considering the effects of the fast particle pressure. The experimental NBI power and beam configuration is prescribed. The plasmas are fuelled by the high energy neutrals injected by the NBI (calculated self-consistently by ASCOT) and by gas fuelling, where the gas inlet locations and time-varying gas puff rates in the model are the same as in the experiment, considering an averaged delay for the arrival of the gas to the vacuum vessel of ~50 ms. The net fuelling of the confined plasma is thus determined by the NBI particle source and the gas puffing and recycling source that is evaluated self-consistently with EDGE2D-EIRENE (neglecting wall D retention effects). Plasma radiation is calculated self-consistently using cooling rates from the ADAS database. The sputtering of C and the re-deposition of C on the plasma-facing components are properly accounted for by EIRENE. Following the approach in [Groth JNM 2015], pumping was simulated by imposing albedos at pump surfaces located in the upper divertor corner regions where the majority of neutral particles escape to the pump. As suggested in [Kotov PPCF 2008], a constant pump albedo is prescribed that is calibrated in the L-mode phase and then kept fixed with time (of value 0.97 in these simulations).

In the two JET discharges subject to detailed modelling (see Fig. 1), the plasma is initially ohmically heated and in the L-mode regime for t < 9 s. For t > 9 s, NBI heating is ramped to the nominal value of ~20 MW within ~0.2 s, which leads to the triggering of an L-H transition at t ~ 9.3 s. In addition, the deuterium gas puff rate is increased from ~10^{22} s^{-1} for t < 9 s to ~2.5-3.5·10^{22} s^{-1} for t > 9 s in these discharges. After the L-H transition, the density starts to increase rapidly in the edge region leading to the formation of a hollow density profile with higher densities at the top of the ETB than in the plasma centre. The hollowness of the density profile is maintained for several confinement times and disappears, usually with the appearance of the first sawtooth. This behaviour is typical for higher current JET H-mode discharges as they naturally have higher plasma densities, which leads to peripheral NBI power and particle deposition [Loarte NF 2013]. The average density and plasma energy increase quickly in the ELM-free phase after the L-H transition and they continue to rise at reduced rates when the MHD stability limit is reached in the pedestal and the plasma enters the ELMy H-mode regime (t > ~9.7-9.8 s) until stationary conditions are obtained. Core radiation remains at a fairly low level of ~1-2 MW, and the core plasmas have relatively low carbon impurity concentration with Z_{eff} ~ 1.4-1.6. In the stationary H-mode phase the ratio of total input power to the power required to access the H-mode (P_{L-H}), according to the scaling in [Martin JPhys 2008], is P_{tot}/P_{L-H} < 2, similar to ITER Q_{DT} = 10 plasma conditions [Hawryluk NF 2009].

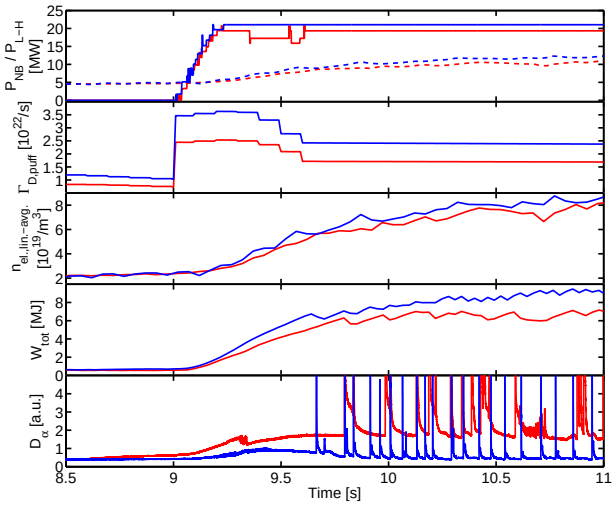

Figure 1: From top to bottom: Time evolution of NBI power (solid) and L-H transition threshold power (dashed, Martin scaling), D gas puff rate, line-averaged electron density, total plasma energy, D_α emission from the outer divertor for the transition phase from L-mode to stationary H-mode conditions in JET discharges #79668 3.8MA/3.0T (blue) and #79688 3.5MA/2.8T (red).

3.1. L-H transition in JET discharge #79688:

Main simulation results and comparisons with measurement data for the transition from L-mode to stationary H-mode in JET discharge #79688 are shown in Figs. 2-10. The simulations for NBI

heating in #79688 have been performed with the ASCOT code that takes into account the slowing-down time of fast particles, which is important to accurately determine the net power in the initial stages of plasma evolution after the start of NBI heating. The SOL geometry was evolved with time (in agreement with EFIT predictions), as the strike point on the outer target moves away from the pump location during the transition to stationary H-mode in this discharge, which has a significant impact on the pumping efficiency and the density evolution.

Good overall agreement between modelling predictions and the available plasma measurements is obtained. As indicated in Fig. 6, the slow inward propagation of a peak in density at the edge, which is formed after the L-H transition, is well reproduced with the GLF23 anomalous core transport model. The level of particle transport is predicted to be very low despite the appearance of positive density gradients, which explains the very slow equilibration in the core density. The good agreement in the core density evolution after the transition to H-mode confirms that particle transport in this regime can be well described and understood by standard ITG/TEM microturbulence theory based models, as was recently demonstrated in [Baiocchi NF 2015].

In stationary H-mode, the agreement in the evolution of core temperature, energy and internal inductance could probably be further improved with consideration of sawteeth, as indicated in Figs. 3-4 where additional time traces are shown for a short demonstration run for t = 10.5-11 s with discrete sawtooth events (described by Kadomtsev model [Kadomtsev SovJPP 1975]). As mentioned before, the effect of sawteeth in the transition phase to stationary H-mode, which is of main interest here, is negligible though, as sawteeth are almost absent in that period.

As can be seen in Fig. 3, the predicted neutral flux through the separatrix does not increase and even starts to decrease after the L-H transition ($\Gamma_{Dneut,sep}$ < ~1.0-1.5$10^{22}$/s), although the applied gas puff rate is more than doubled. This is caused by an increased power flux from the core and an increase in density in the SOL (see Fig. 7) which leads to an increased fraction of neutral particles being ionised in the SOL. The increase in the gas puff rate is therefore not directly responsible for the rise of the edge density after the L-H transition via enhanced core fuelling by cold neutrals, which makes the confined plasma properties modelled to be relatively insensitive to the pump efficiency and detail of edge fuelling conditions.

Both the increase in density and energy after the L-H transition can be reproduced with the assumption of a reduction of anomalous transport depending on P_{net}/P_{L-H} applying λ_χ = 0.20 and λ_D = 0.08 which results in the time evolution of the energy and particle transport coefficients at the separatrix shown in Fig. 5. The edge MHD stability limit leading to the onset of ELMs in the simulations is reached at t ~ 10.05 s. At that time, P_{net}/P_{L-H} ~ 1.6, therefore the anomalous energy transport is still not yet fully suppressed by the L-H transition model applied when the continuous ELM model starts to increase ETB transport. It is important to note that the increase in P_{net} in these discharges is slower than what would be estimated with the injected NBI power since the time required for thermalisation of NB particles has been taken into account. Using other values for λ_χ and λ_D lead to simulations that cannot reproduce accurately the simultaneous change of

plasma density and temperature in the core plasma, ETB and SOL as shown in section 3.2. D_i, χ_e, and χ_i at the separatrix are plotted in Fig. 5.
Integrated modelling of the complete plasma allows us to evaluate quantitatively, whether the changes in plasma transport, which are required to reproduce plasma behaviour in the core and ETB plasmas in the phase from L-mode to high confinement H-mode, describe also the behaviour of the plasma on open flux surfaces (i.e. the SOL), or different assumptions regarding changes in plasma transport are required in this region to describe plasma behaviour in this phase. This is important because SOL transport determines both the magnitude of the power and particle flux densities on PFCs during this phase as well as the edge density and temperature profiles, which in turn determine the degree of edge ionisation of the recycled neutrals and the magnitude of the ionisation source in the ETB.

In view of the abovementioned considerations, the evolution of the edge and SOL density and electron and ion temperature profiles and of the power and particle fluxes to the divertor during the phase from L-mode to high confinement H-mode have been analysed in detail for #79688 for which high quality divertor measurement data is available. Regarding SOL profiles, the uncertainty in the position of the separatrix needs to be taken into account. This has been done by following the approach proposed in [Kallenbach JNM 2005] to determine the separatrix location from the experimentally measured profiles for stationary H-mode conditions and then keeping the difference between the determination of the separatrix position by this scheme and that predicted from equilibrium constant throughout the transition phase from L-mode to high confinement H-mode. This typically leads to electron separatrix temperatures in the range of 100-150 eV and ratios of pedestal densities to separatrix densities of ~ 2.0 for stationary H-mode conditions, which are consistent with findings for JET in [Kallenbach JNM 2005]. With this prescription to determine the separatrix position, the modelled evolution of the ETB and SOL density profiles throughout this phase and electron temperature profiles in the late H-mode phase are in good agreement with experiment as shown in Figs. 7-8. This is not a trivial result as the choice of the energy and particle anomalous transport reduction used in the modelling is dictated by requirements to reproduce the core plasma evolution and this does not necessarily ensure that the predicted edge plasma evolution is in agreement with experiment. Indeed, the good agreement shown in Figs. 7-8 demonstrates that the assumptions used regarding the extension of the ETB transport barrier by few mm into the SOL in H-mode and for the reduction of the transport with increasing P_{net}/P_{L-H} are also appropriate to describe SOL plasma behaviour.

In an attempt to further substantiate the appropriateness of the applied model assumptions for the description of the evolution of SOL plasma conditions, the modelled particle and power fluxes to the divertor have been compared with the measured ones during the transition phase from L-mode to high confinement H-mode. Figs. 9 -10 show comparison, for the outer and inner divertor respectively, of the modelled total power, peak power density and average D_α emission with the experimental measurements. It should be noted that there are no independent measurements of density and temperature by Langmuir probes at the divertor for this discharge and that the comparison for divertor fluxes is restricted to $t > 9.3$ s because due to the changes in magnetic configuration illustrated in Fig. 2, the strike point hits edges of tiles, distorting the divertor power

measurements. From t > 9.8 s ELMs are triggered in experiment and this leads to large spikes in the D_α and power fluxes which are not reproduced by the simulations where a continuous ELM model is used. As shown in Fig. 9, the simulated total power, peak power flux and average particle flux (D_α) to the outer divertor are in reasonably good agreement with the model. Some of the discrepancies are associated with diagnostic limitations. For instance, for the total outer divertor power load, the simulations evaluate the total power arriving at the outer divertor, whereas the measurement only includes those in the field of view of the infrared camera diagnostic. The latter cannot measure power fluxes near the outer corner of the divertor and this explains, why the simulated total power is larger than in the experiment although the peak power flux is in good agreement. The good agreement between the simulated and measured power and particle fluxes again confirms that the assumptions regarding SOL transport during the L-H transition and of the reduction of anomalous transport in the H-mode transient phase with P_{net}/P_{L-H} is not only appropriate to describe the evolution of plasma density and temperature in the core+ETB+SOL but also to describe the evolution of the power and particle fluxes during this phase. It should be noted, however, that the agreement between simulations and measurements is worse for the inner divertor target. The simulations overestimate the peak power fluxes and under-estimate the particle fluxes at the inner divertor compared to experimental measurements. This is a well-known deficiency of edge plasma simulations that do not include the effect of plasma drifts, etc. (cf. [Chankin PPCF 2015] and references therein). An improvement in the prediction of plasma conditions near the inner target may therefore only be achieved by consideration of more sophisticated SOL transport models, which is outside the scope of this paper.

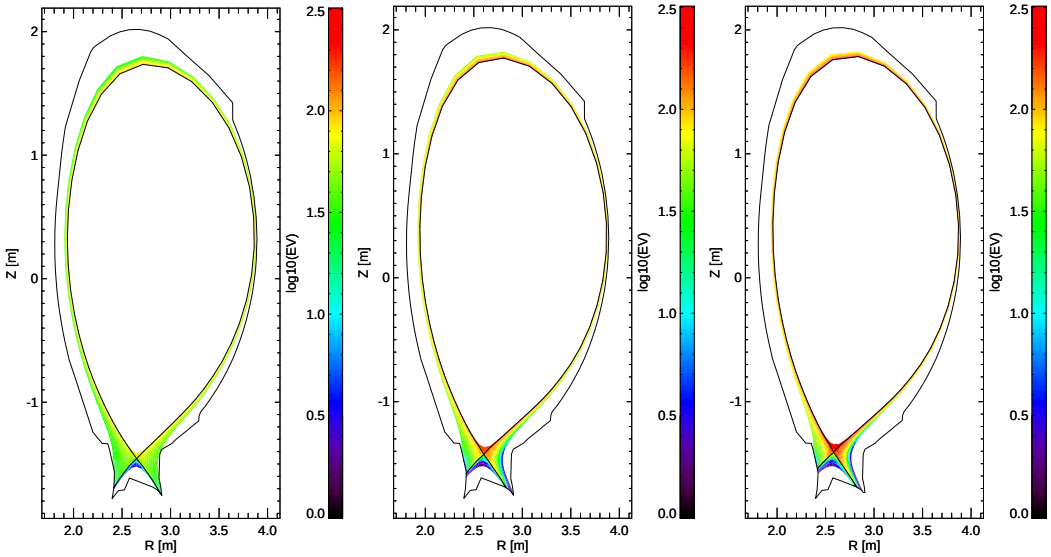

Figure 2: Contour plots of the ion temperature in the SOL for t ~ 8.75 s, t ~ 9.50 s and t ~ 10.75 s for #79688, illustrating the variation in SOL geometry and the movement in strike point position during the transition from L-mode to stationary H-mode in this discharge.

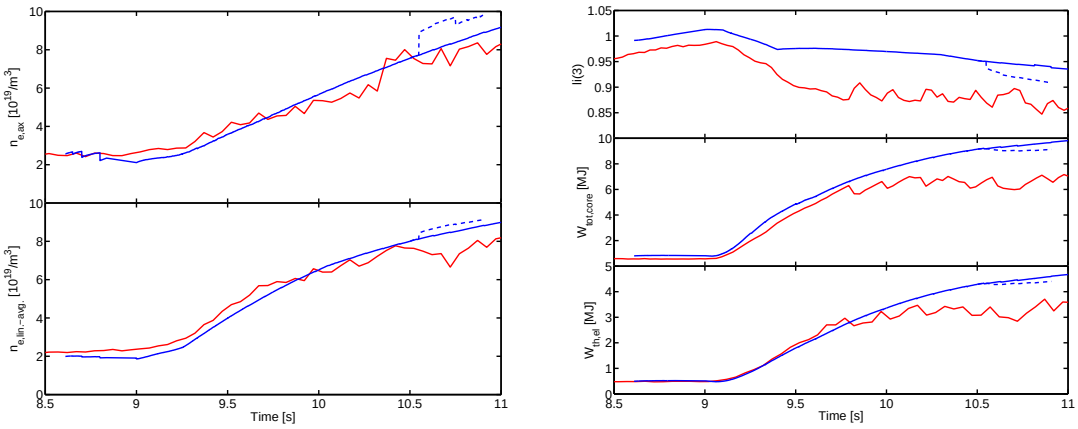

Figure 3: Measured (red) vs. simulated (blue, dashed: with sawteeth for t > 10.5 s) time evolution of main plasma quantities for the transition to high quality H-mode in JET discharge #79688. Left: electron density on axis, line-averaged electron density. Right: plasma internal inductance, total energy content, thermal electron energy content.

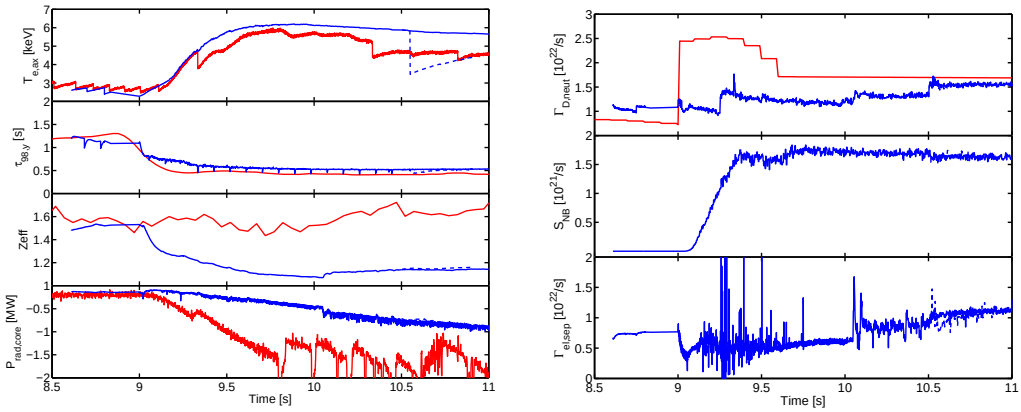

Figure 4: Left: Measured (red) vs. simulated (blue, dashed: with sawteeth for t > 10.5 s) time evolution of the electron temperature on axis, energy confinement time, Z_{eff} and core plasma radiation. Right: D gas puff applied in the experiment and modelling (red) vs. simulated D neutral influx at the separatrix (blue), NBI particle source rate, ion outflux across the separatrix, for the transition to high quality H-mode in JET discharge #79688.

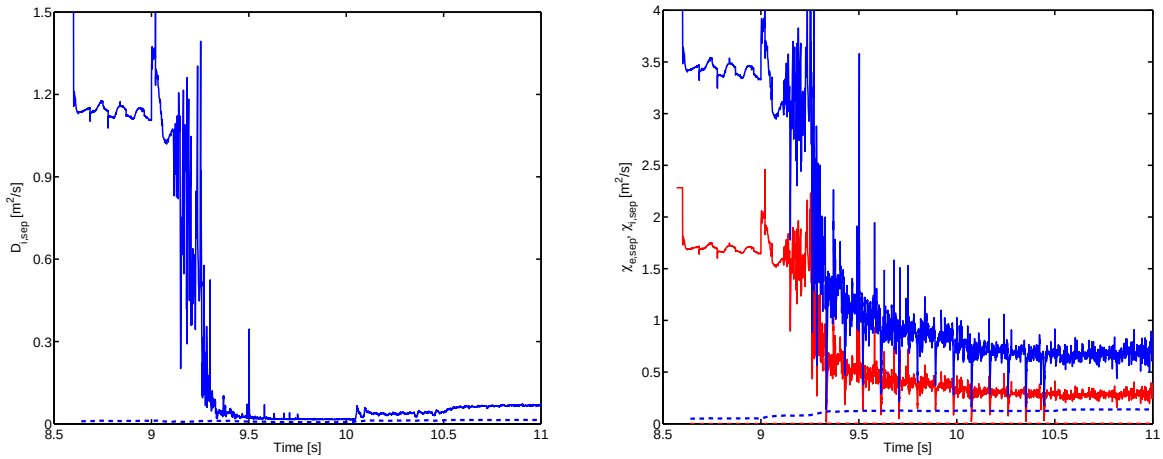

Figure 5: Left: time evolution of D particle diffusivity, right: time evolution of electron (red) and ion (blue) heat conductivity at the separatrix, for the transition to high quality H-mode in JET discharge #79688. Solid: total, dashed: neoclassical diffusivity / conductivity.

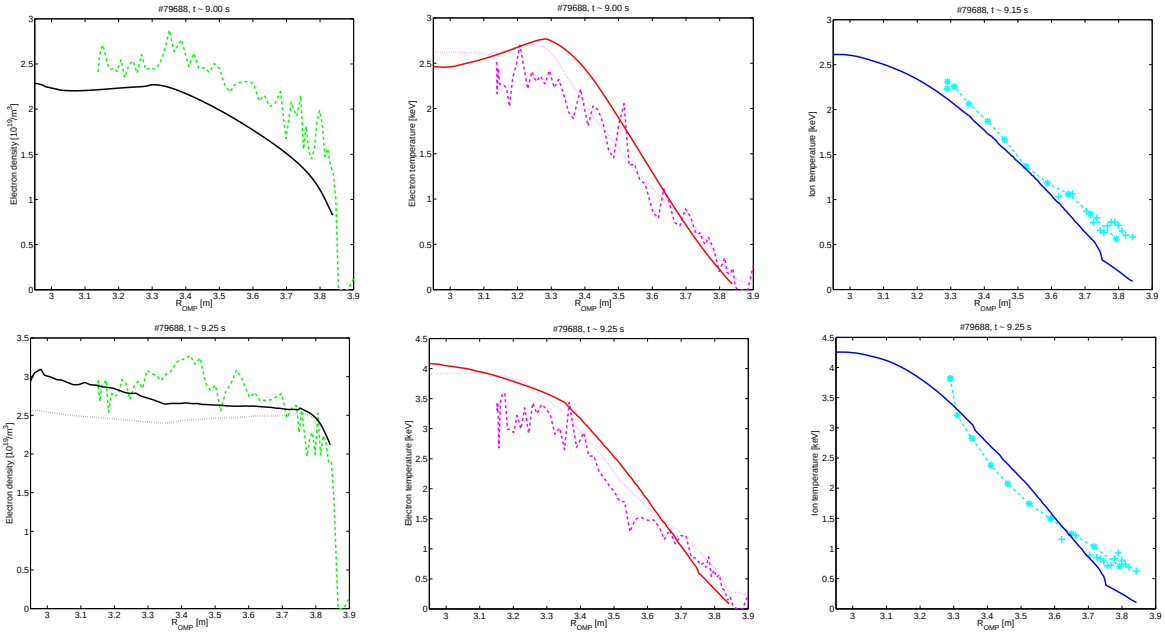

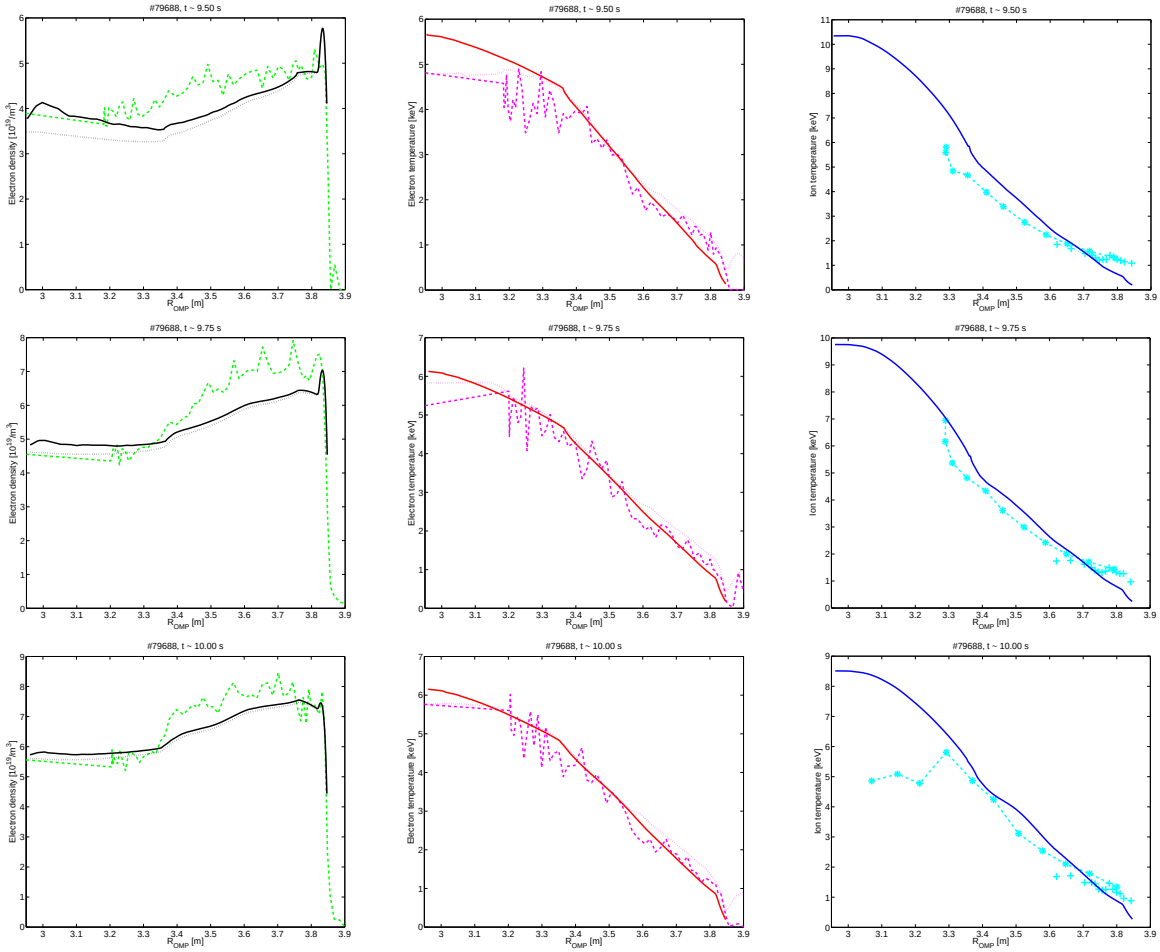

Figure 6: Left: electron density, black dashed: simulated thermal n_e, black solid: simulated total n_e, green dashed: n_e from high resolution Thomson scattering measurement; middle: electron temperature, red: simulated T_e, magenta dashed: T_e from high resolution Thomson scattering measurement, magenta dotted: T_e from ECE diagnostics; right: ion temperature, blue: simulated T_i, cyan dashed: T_i from CXRS diagnostics, cyan dotted: T_i from edge CXRS diagnostics. Profiles are shown for the transition to high quality H-mode in JET discharge #79688 at t ~ 9 s/9.15 s, 9.25 s, 9.5 s, 9.75 s, 10 s (from top to bottom) as function of the major radius on the outer mid-plane.

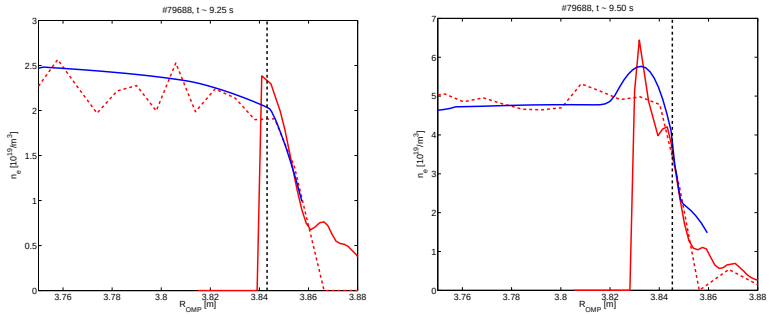

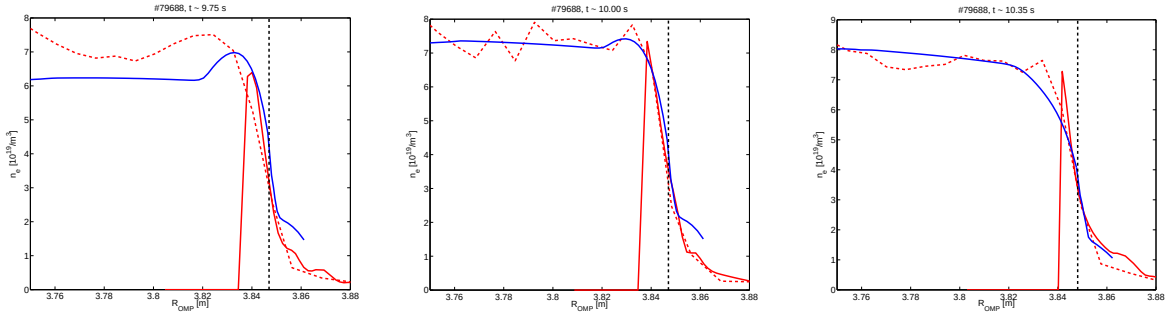

Figure 7: Measured (red, dashed: high resolution Thomson scattering data, solid: Li beam diagnostics) vs. simulated (blue, solid) electron density in the edge and SOL along the outer mid-plane at t ~ 9.25 s (early H-mode), 9.5 s (density ramp phase), 9.75 s (late ELM free H-mode phase), 10 s (early stationary ELMy H-mode phase), and 10.35 s (stationary ELMy H-mode) in JET discharge #79688. The LCFS location is indicated by dashed lines.

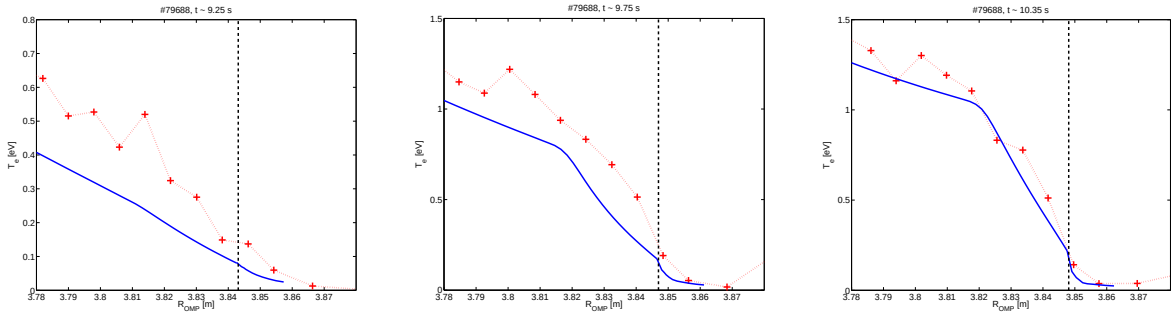

Figure 8: Measured (red, dotted: high resolution Thomson scattering data) vs. simulated (blue, solid) electron temperature in the edge and SOL along the outer mid-plane at t ~ 9.25 s (early H-mode), 9.75 s (late ELM free H-mode phase), and 10.35 s (stationary ELMy H-mode) in JET discharge #79688. The LCFS location is indicated by dashed lines.

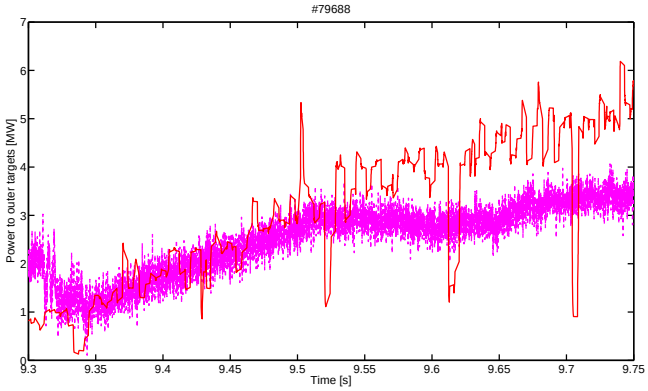

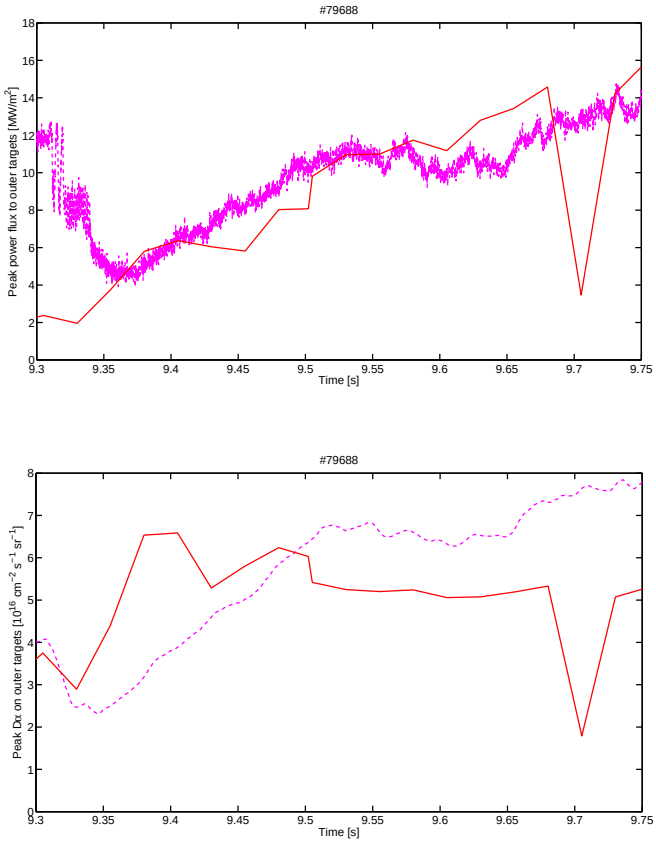

Figure 9: From top to bottom: Time evolution of measured (dashed) vs. simulated (solid) power to outer target, peak power flux to outer target and peak D_α signal near the outer target for the transition to high quality H-mode in JET discharge #79688.

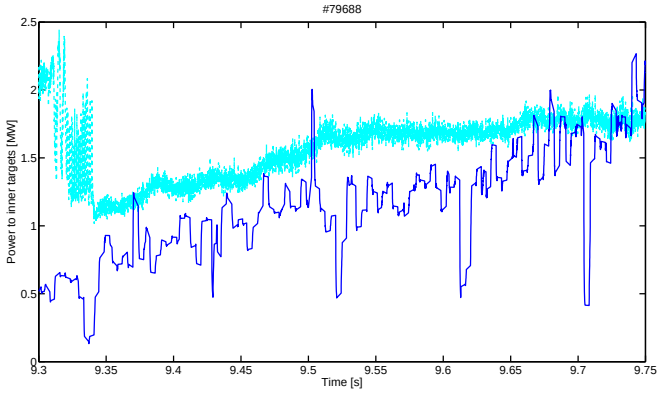

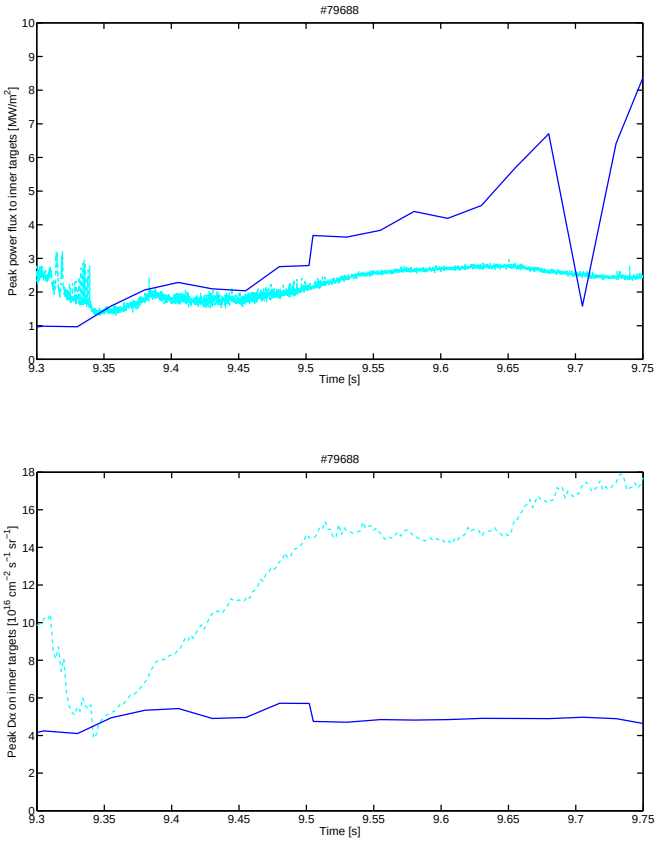

Figure 10: From top to bottom: Time evolution of measured (dashed) vs. simulated (solid) power to inner target, peak power flux to inner target and peak D_α signal near the inner target for the transition to high quality H-mode in JET discharge #79688.

3.2. Sensitivity of the results to the values of λ_χ, λ_D:

The reduction of anomalous transport at the ETB and near SOL in the JINTRAC simulations depends on the empirical constants λ_χ, λ_D. The results in section 3.1 correspond to the specific choice $\lambda_\chi = 0.20$, $\lambda_D = 0.08$, which is found to reproduce best the experimental data but that leads to a different reduction of the anomalous transport for particles and energy in the transient H-mode phase as P_{net}/P_{L-H} increases. It is therefore important to substantiate this choice and to demonstrate that this is the optimum one to reproduce JET experimental results before applying the models to ITER. In first place, it should be noted that good H-mode confinement requires the edge power flow to exceed the H-mode threshold power by a given threshold so that, typically, $P_{net}/P_{L-H} > 1.3$-1.5 is required for high confinement H-modes; for lower powers low confinement H-modes and Type III ELMs are observed at JET [Sartori PPCF 2004]. In the JINTRAC model and in the experiment, the achievement of high H-mode confinement is linked with the reduction of the transport in the ETB and the formation of a high pressure gradient region in the ETB. As the reduction of anomalous transport in the JINTRAC model is given by $\exp((P_{net}-P_{L-H})/(\lambda_{\chi/D}\cdot P_{L-}$

$_H$)), this implies that λ_χ and λ_D must have values of the order of ~ 0.1 so that P_{net}/P_{L-H} >1.3-1.5 provides a sizeable anomalous transport reduction (exp(-3) to exp(-5)). The ratio λ_χ/λ_D then needs to be adjusted to take into account possible differences in the P_{net}/P_{L-H} level required to achieve a strong suppression in particle versus energy transport.
In the JET experiments that have been analysed for this study, it is found that the evolution of density and temperature gradients occurs on different timescales after the L-H transition. This can be due to the fact that anomalous energy and particle transport do not decrease in the same magnitude as the plasma evolves towards high confinement H-mode conditions but also to the fact that power and particle fluxes at the edge have different origins and do not evolve in the same way after the L-H transition. The power flux arriving from the plasma core is continuously increasing while the effective particle source due to ionisation of recycling neutrals in the confined plasma remains roughly constant or may even be reduced in this phase in JET, as the edge neutral fuelling efficiency decreases. Similarly the core plasma sources by NBI also change as the NBI particle deposition profile becomes more prominent at the edge due to the poorer beam penetration as the edge density increases. It is therefore important to perform a sensitivity study for the dependence of the evolution of plasma density and temperature in the access phase to high performance H-mode on the reduction of anomalous energy and particle transport following the H-mode transition, described by λ_χ and λ_D in the JINTRAC modelling approach.

In Figs. 11-15, the results of JINTRAC simulations with $\lambda_\chi = 0.20$, $\lambda_D = 0.08$ and $\lambda_\chi = \lambda_D = 0.10$ are compared with measurements of plasma parameters for the transition to stationary H-mode in #79688. Indeed, as mentioned above the experimental behaviour is well reproduced with $\lambda_\chi = 0.20$, $\lambda_D = 0.08$ (possibly a fine tuning of these values could improve further the code-experiment agreement), while the choice of $\lambda_\chi = \lambda_D = 0.1$ fails to reproduce the main features of the experiment. In particular, the core+ETB plasma density evolution and the peak heat loads and D_α emission at the outer divertor are considerably underestimated by modelling with $\lambda_\chi = \lambda_D = 0.1$, in which both energy and particle anomalous transport decrease in the same fashion with P_{net}/P_{L-H}, compared to $\lambda_\chi = 0.20$ and $\lambda_D = 0.08$, in which anomalous energy transport decreases more gently with P_{net}/P_{L-H} than anomalous particle transport. Differences in the cold neutral influx to the core are not responsible for the underestimation of the core density increase with $\lambda_\chi = \lambda_D = 0.1$. Compared to the case with $\lambda_\chi = 0.20$, $\lambda_D = 0.08$, the neutral influx is even slightly increased by $\sim 2 \cdot 10^{21}$/s on average in the density ramp phase due to less efficient neutral ionisation in the SOL which is a consequence of a reduced power flux at the separatrix at lower λ_χ in the transition to stationary H-mode.

This modelling finding of an asymmetry in the reduction in χ versus D in the H-mode transient phase, evaluated by analysing the edge density and temperature profiles, is also supported by the direct evaluation of the experimental effective diffusivities as shown in Fig. 16. The reduction in effective particle diffusivity after the L-H transition is larger than the relative reduction in effective heat diffusivity, which can only be reproduced in the JINTRAC model by assuming a ratio $\lambda_\chi/\lambda_D > 1.0$. It should be noted, however, that calculation of the experimental effective diffusivities is not completely independent from the JINTRAC simulation results as the computed

power and particle fluxes near the separatrix have been taken into account in these calculations in addition to the measured edge density and temperature profiles.

The observed differences between λ_χ and λ_D can be interpreted in various ways. This difference may indicate that long wavelength turbulence is reduced first in the ETB in the transition to high quality H-mode. Both χ_i and D would then be reduced much earlier than χ_e. According to the evolution of the effective edge ion heat diffusivity inferred from measurement data as shown in Fig. 16, that may not be the case, as $\chi_{i,eff}$ appears to be reduced at a similar scale as the electron heat diffusivity. It should be noted though that edge CXRS diagnostic measurement data were used for the calculation of $\chi_{i,eff}$ where ion temperature values in the order of 1 keV are given for the outermost measured location in H-mode. As T_i at the separatrix is typically found to be much lower in a temperature range more comparable with $T_{e,sep}$, one cannot exclude the possibility that a narrow region near the separatrix with increased gradient in T_i is formed after the L-H transition similar to the localised formation of high density gradients near the separatrix as illustrated in Fig. 7. This region might just not have been captured by the edge CXRS diagnostics. If such a region exists, the relative reduction in $\chi_{i,eff}$ with time might actually better correspond to λ_D rather than λ_χ. Thus, the possibility of different time scales for the reduction of long vs. short wavelength turbulence cannot yet be discarded. An alternative explanation is that a phase shift in turbulent density versus velocity perturbations could lead to reduced net particle transport compared to net energy transport. The latter may also be associated with the formation of an anomalous inwards pinch in the ETB in H-mode plasmas [Willensdorfer NF 2013]. Investigating the exact cause of the discrepancy in λ_χ and λ_D is out of the scope of this paper and will be the subject of further studies.

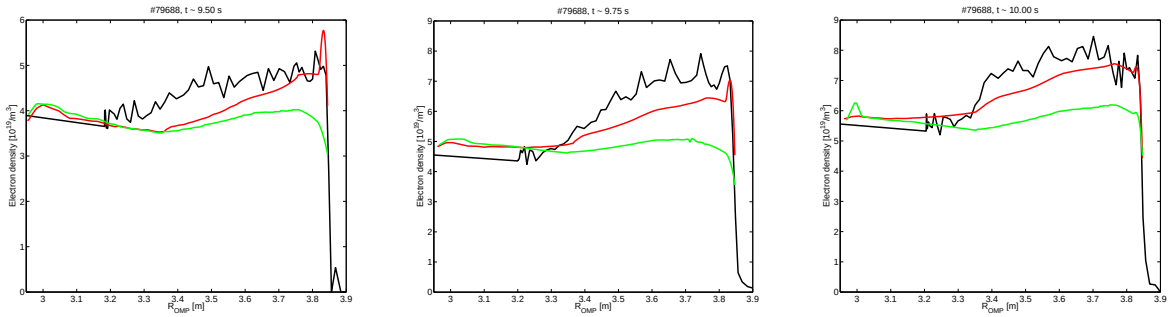

Figure 11: Measured (black, high resolution Thomson scattering data) versus simulated (red/green) total electron density profiles obtained with λ_χ = 0.20, λ_D = 0.08 (red) and λ_χ = 0.10, λ_D = 0.10 (green) at t ~ 9.5 s (left, density ramp phase), 9.75 s (late ELM free H-mode phase), and 10.0 s (early stationary ELMy H-mode phase) for JET discharge #79688.

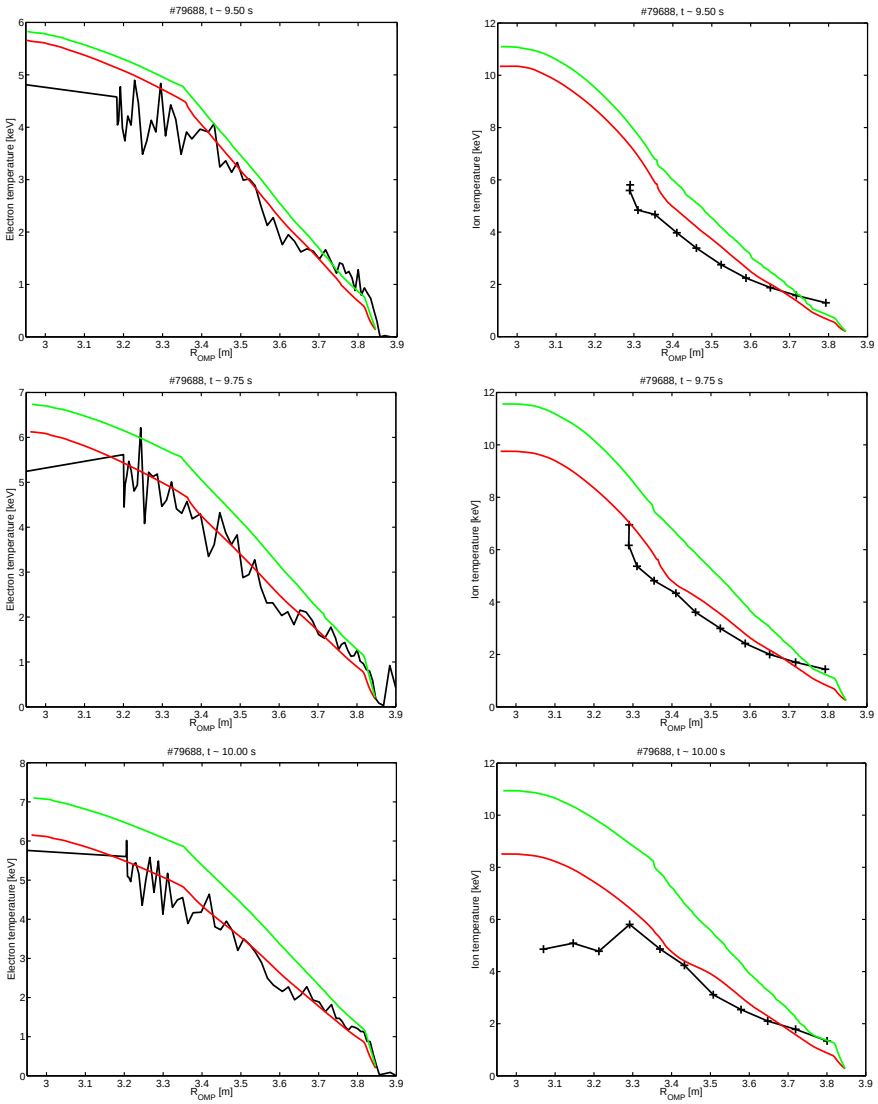

Figure 12: Measured (black, high resolution Thomson scattering / CXRS diagnostics data) versus simulated (red/green) electron (left) and ion (right) temperature profiles obtained with $\lambda_\chi = 0.20$, $\lambda_D = 0.08$ (red) and $\lambda_\chi = 0.10$, $\lambda_D = 0.10$ (green) at t ~ 9.5 s (top, density ramp phase), 9.75 s (bottom, late ELM free H-mode phase), and 10.0 s (early stationary ELMy H-mode phase) for JET discharge #79688.

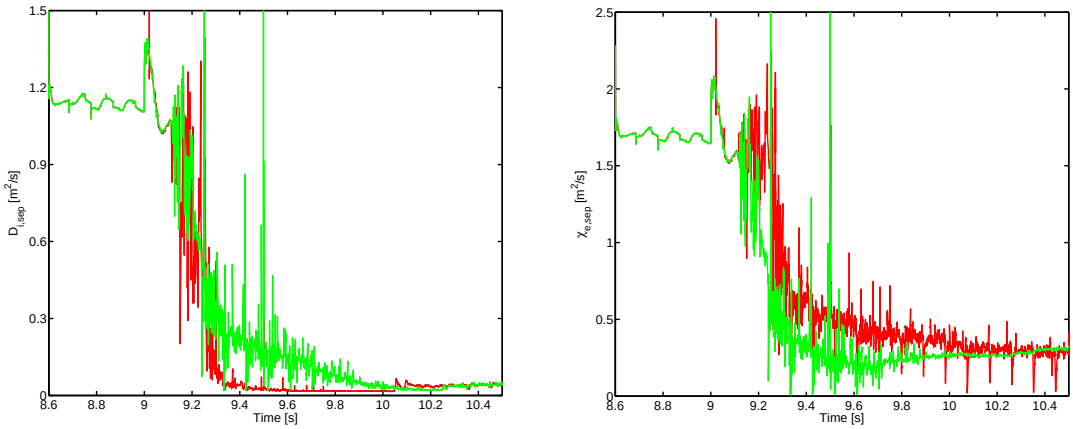

Figure 13: Left: time evolution of D particle diffusivity, right: time evolution of electron heat conductivity at the separatrix, obtained with $\lambda_\chi = 0.20$, $\lambda_D = 0.08$ (red) and $\lambda_\chi = 0.10$, $\lambda_D = 0.10$ (green) for the transition to high quality H-mode in JET discharge #79688.

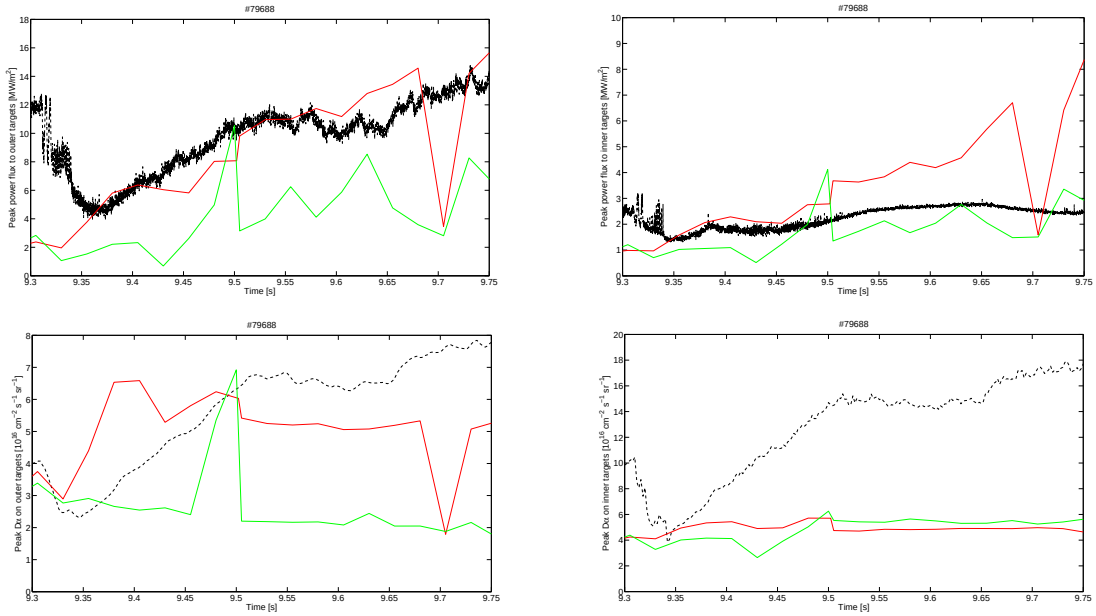

Figure 14: From top to bottom: Time evolution of measured (black) versus simulated (red/green) peak power flux and D_α emission from the divertor target obtained with $\lambda_\chi = 0.20$, $\lambda_D = 0.08$ (red) and $\lambda_\chi = 0.10$, $\lambda_D = 0.10$ (green) for outer (left) and inner (right) divertor targets for the transition to high quality H-mode in JET discharge #79688.

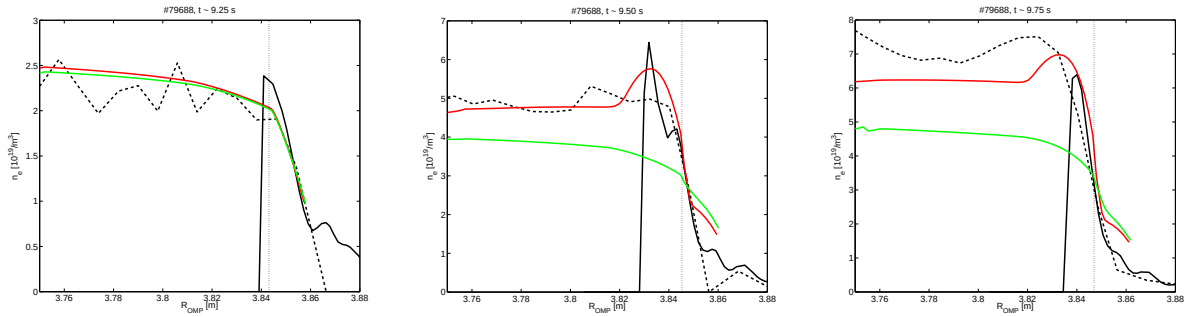

Figure 15: Measured (black, dashed: high resolution Thomson scattering data, solid: Li beam diagnostics) versus simulated (red/green, solid) electron density in the edge and SOL along the outer mid-plane obtained with λ_χ = 0.20, λ_D = 0.08 (red) and λ_χ = 0.10, λ_D = 0.10 (green) at t ~ 9.25 s (early H-mode), 9.5 s (density ramp phase), 9.75 s (late ELM free H-mode phase), in JET discharge #79688. The LCFS location is indicated by dotted lines.

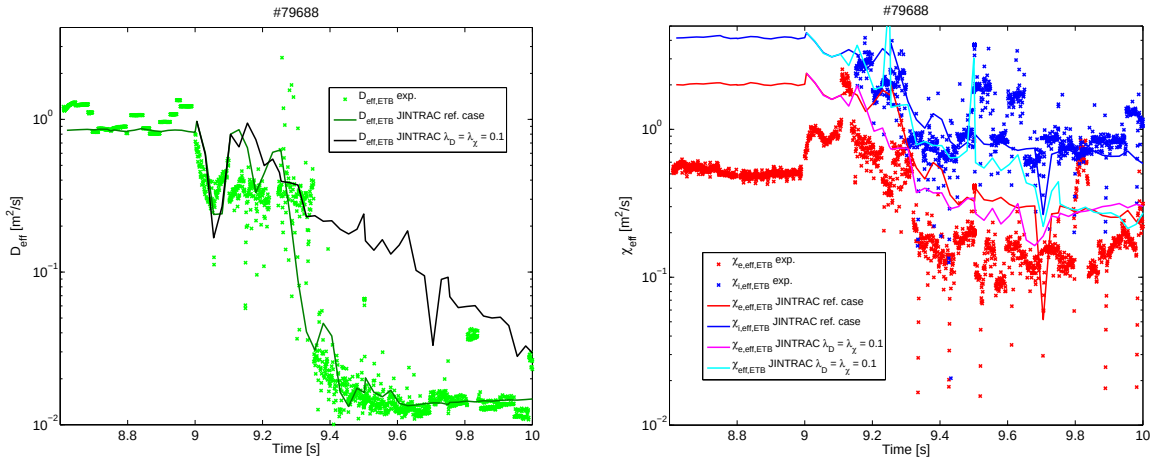

Figure 16: Time evolution of measured (crosses, HRTS / ECE / edge CXRS diagnostics) versus simulated (solid) effective particle (left, green/black), electron heat (right: red/magenta) and ion heat (right: blue/cyan) diffusivities in the ETB near the separatrix obtained with the reference choice of parameters λ_χ = 0.20, λ_D = 0.08 (green/red/blue) and λ_χ = 0.10, λ_D = 0.10 (black/magenta/cyan) for JET discharge #79688.

3.3. L-H transition in JET discharge #79668

In order to evaluate the robustness of the findings for # 79688, simulations have been performed for another JET ITER-like plasma (#79668) with the same modelling assumptions (i.e. λ_χ = 0.20, λ_D = 0.08). The discharge #79668 has several advantages from the point of modelling (the divertor geometry does not change significantly through the L-mode to stationary H-mode phase, edge impurity density measurements are available) but also disadvantages regarding plasma measurements due to the divertor geometry (no divertor power and particle fluxes are available). The results of the simulations are shown in Figs 17-23 with satisfying overall agreement between

simulations and experimental measurements. This includes the edge density and temperature behaviour and the relaxation of the hollow density profiles. However, the predicted hollowness of the core density profile in the later phase of the transition to stationary H-mode is less pronounced and the disagreement with the measured hollowness is larger compared to #79688. As in the case of #79688, the predicted neutral flux through the separatrix does not increase and even starts to be reduced after the L-H transition ($\Gamma_{Dneut,sep} < \sim 10^{22}$/s), although the applied gas puff rate is roughly tripled, due to enhanced ionisation of recycling neutrals in the SOL during this phase. The sensitivity of the influx of recycled neutrals into the confined plasma to the applied gas puff has been assessed by varying the gas puffing level in the modelling and was found to be weak provided that detachment conditions remain unchanged. Increasing the gas puffing rate to levels twice larger than in the experiment only leads to changes in the average plasma density of ~10 %. Similarly, the results of simulations are rather insensitive to uncertainties for the prescription of the pump efficiency. For instance, the average core density increases only by ~ 5% if the pump albedo is modified such that the pump efficiency is reduced by a factor of 2.

The good edge carbon density measurements in this discharge allow a comparison between the measured and predicted carbon density profiles. Overall impurity particle transport is satisfactorily described by the simulations, the predicted Z_{eff} in the core plasma and core radiation agree roughly with measurement data (see Fig. 18), although the impurity concentration may be underestimated especially in the early H-mode phase, indicating that a noticeable concentration of impurities other than C may also be present which are not taken into account in the simulations. Both absolute values and the relative evolution with time of the carbon impurity density are in reasonable agreement with the measured ones (see Fig. 22). In particular the change of shape of the carbon density profile as the plasma enters the H-mode and the ETB appears is well predicted by the model, although details in the profile shape evolution such as the time evolution of the C profile barycentre are reproduced less accurately. Like for main ions, the carbon density builds up quickly at the plasma edge due to the increased C sputtering source with increasing power and the neoclassical inward pinch in the pedestal. Since the anomalous transport for C predicted by GLF-23 is as small as that for D in the core, the C density profile becomes hollow soon after the L-H transition (t ~ 9.3-9.4 s). It then remains peaked at the plasma periphery, as the central carbon density increases very slowly with time.
As for #79688, the time evolution of effective edge diffusivities and heat conductivities appears to be well described with the choice $\lambda_\chi = 0.20$, $\lambda_D = 0.08$ as shown in Fig. 23. Since the edge barrier in ion temperature measured by the edge CXRS diagnostics is well visible in #79668, the calculated effective ion heat conductivities may be more accurate than for #79688. Although CXRS data are only available for the NB heating phase and $\chi_{i,eff}$ could only be calculated for the H-mode phase, the conclusion can be drawn that χ_i indeed seems to scale in the same way as χ_e rather than D_i. If it did scale with D_i, extreme ion heat conductivites of $\chi_i > 10$ m^2/s would need to be present in L-mode, or the drop in $\chi_{i,eff}$ for increasing P_{net}/P_{L-H} would need to be more pronounced. It is thus unlikely that the difference in λ_χ and λ_D is caused by a faster reduction in long wavelength turbulence as speculated in the previous subsection.

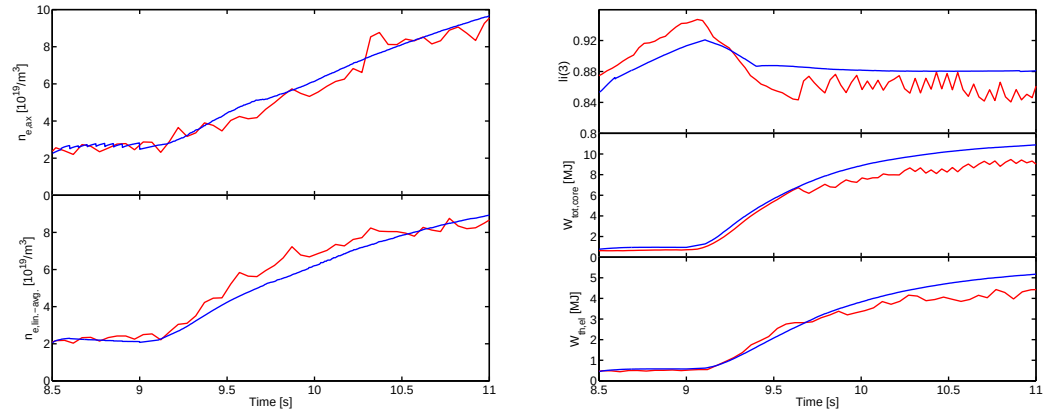

Figure 17: Measured (red) vs. simulated (blue) time evolution of main plasma quantities for the transition to high quality H-mode in JET discharge #79668. Left: electron density on axis, line-averaged electron density. Right: plasma internal inductance, total energy content, thermal electron energy content.

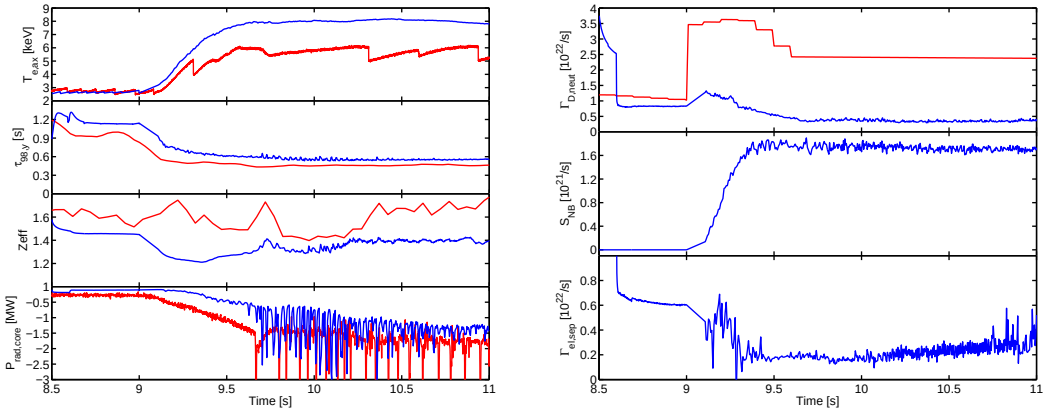

Figure 18: Left: Measured (red) vs. simulated (blue) time evolution of the electron temperature on axis, energy confinement time, Z_{eff} and core plasma radiation. Right: D gas puff applied in the experiment and modelling (red) vs. simulated D neutral influx at the separatrix (blue), NBI particle source rate, ion outflux across the separatrix, for the transition to high quality H-mode in JET discharge #79668.

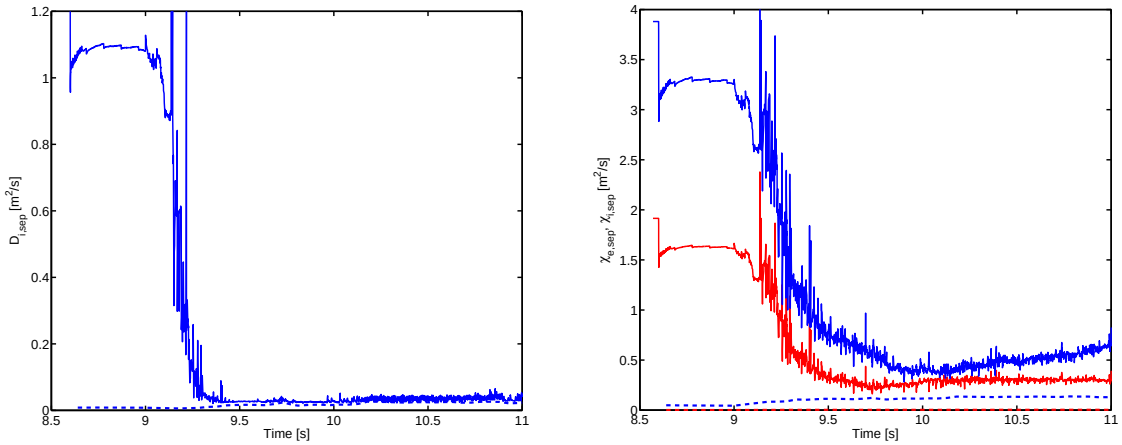

Figure 19: Left: time evolution of D particle diffusivity, right: time evolution of electron (red) and ion (blue) heat conductivity at the separatrix, for the transition to high quality H-mode in JET discharge #79668. Solid: total, dashed: neoclassical diffusivity / conductivity.

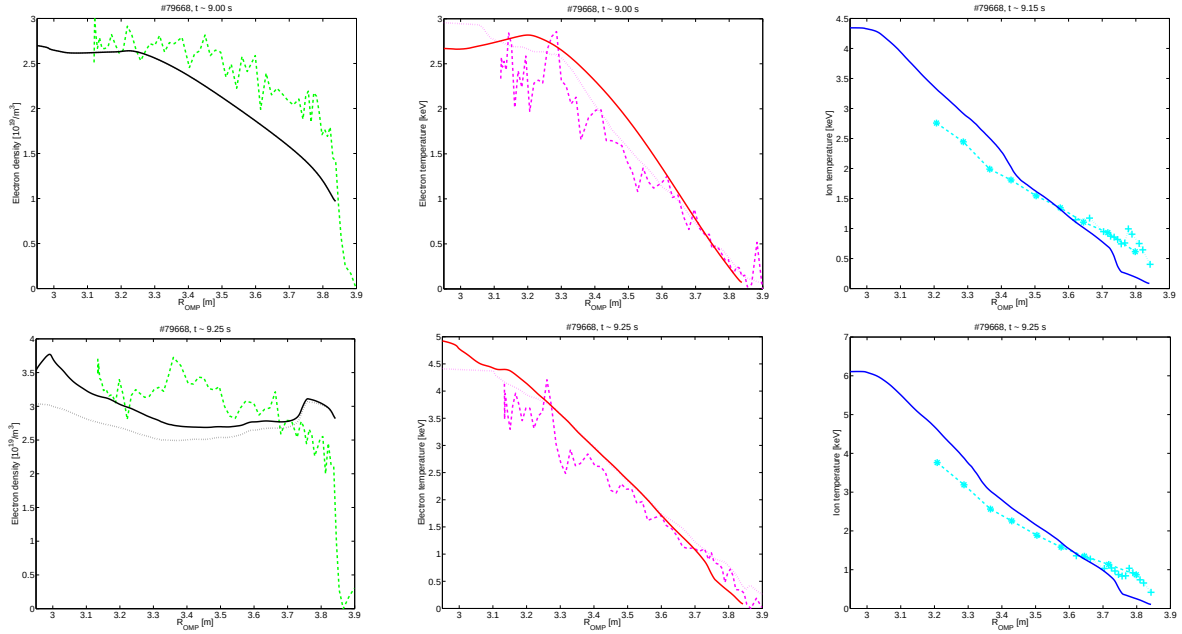

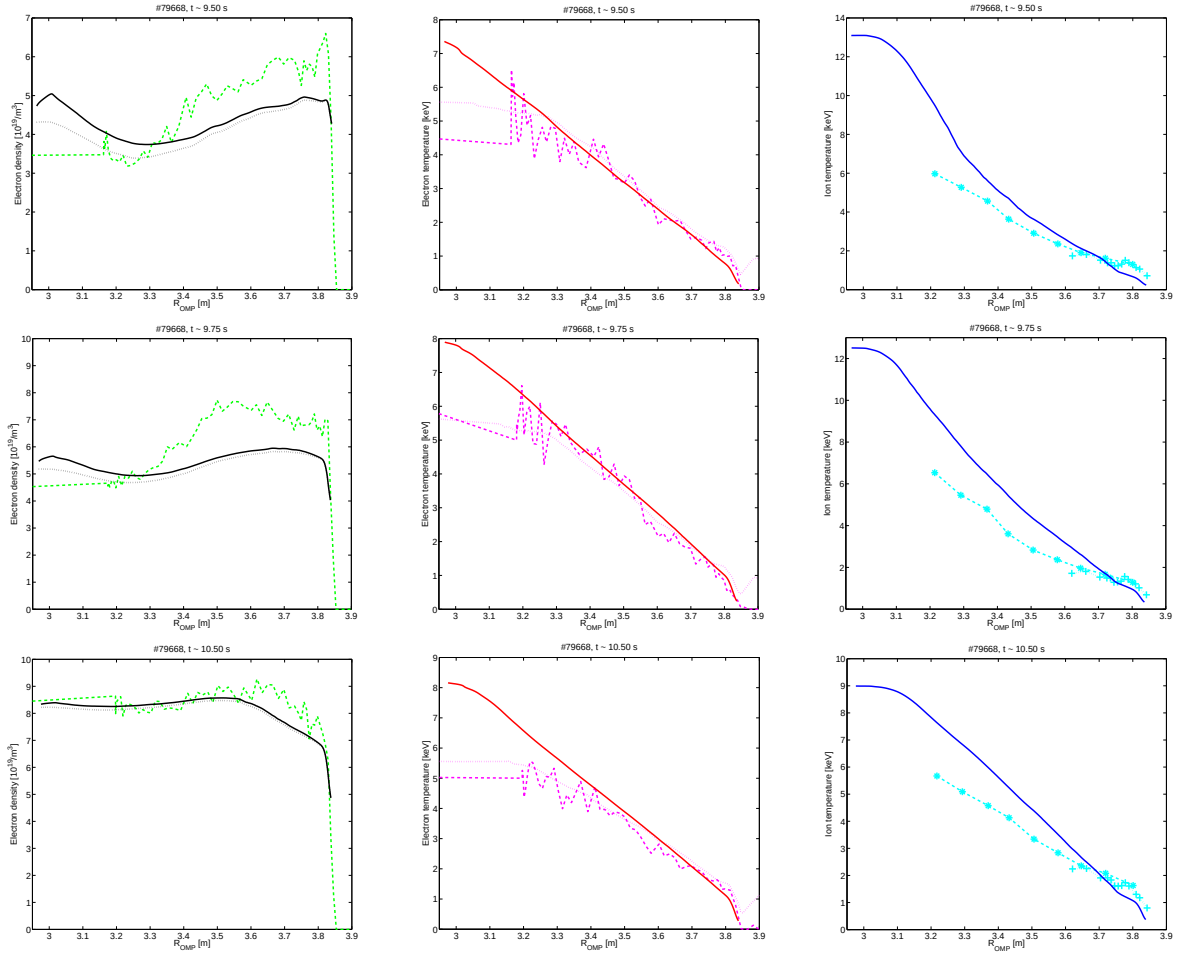

Figure 20: Left: electron density, black dashed: simulated thermal n_e, black solid: simulated total n_e, green dashed: n_e from high resolution Thomson scattering measurement; middle: electron temperature, red: simulated T_e, magenta dashed: T_e from high resolution Thomson scattering measurement, magenta dotted: T_e from ECE diagnostics; right: ion temperature, blue: simulated T_i, cyan dotted: T_i from edge CXRS diagnostics. Profiles are shown for the transition to high quality H-mode in JET discharge #79668 at t ~ 9 s/9.15 s, 9.25 s, 9.5 s, 9.75 s, 10.5 s (from top to bottom) as function of the major radius on the outer mid-plane.

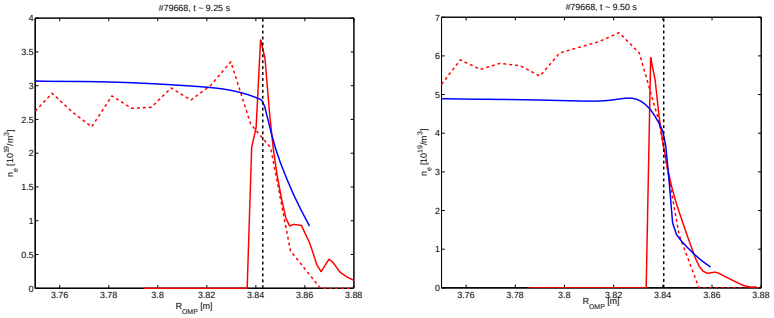

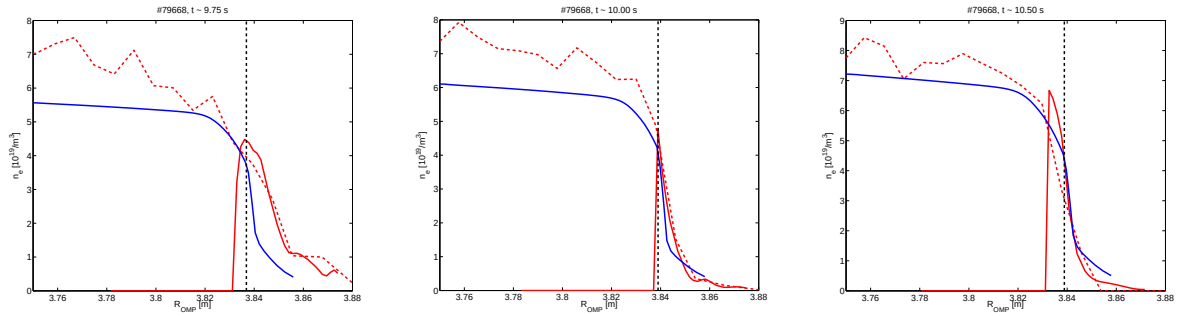

Figure 21: Measured (red, dashed: high resolution Thomson scattering data, solid: Li beam diagnostics) vs. simulated (blue, solid) electron density in the edge and SOL along the outer mid-plane at t ~ 9.25 s (early H-mode), 9.5 s (density ramp phase), 9.75 s (late ELM free H-mode phase), 10 s (early stationary ELMy H-mode phase), and 10.50 s (stationary ELMy H-mode) in JET discharge #79668. The LCFS location is indicated by dashed lines.

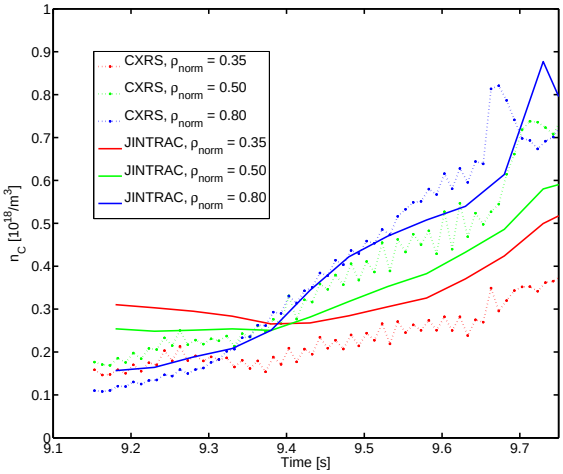

Figure 22: Time evolution of measured (dotted, CXRS measurement) vs. simulated (solid) C density at various locations (red: ρ_{norm} = 0.35, green: ρ_{norm} = 0.50, blue: ρ_{norm} = 0.80) for the ELM free phase in the transition to high quality H-mode in JET discharge #79668.

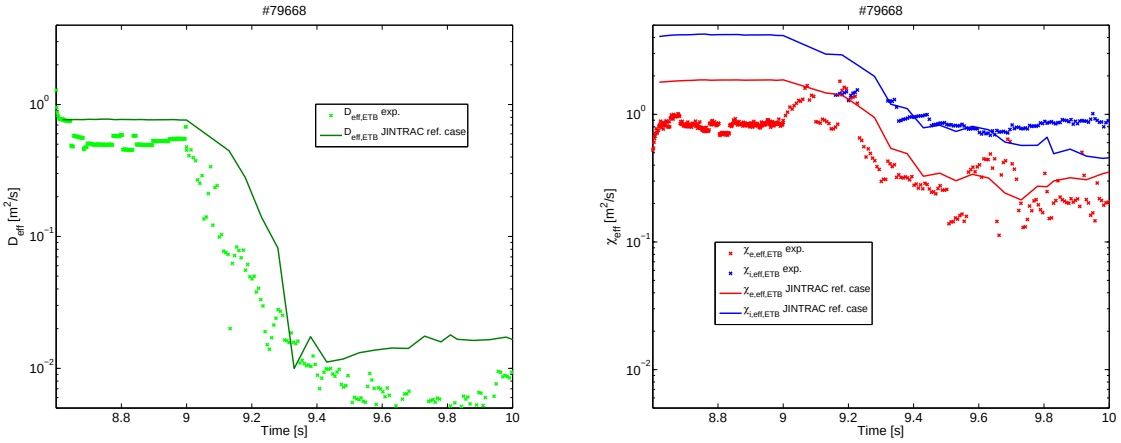

Figure 23: Time evolution of measured (crosses, HRTS / ECE / edge CXRS diagnostics) versus simulated (solid) effective particle (left, green), electron heat (right, red) and ion heat (right, blue) diffusivities in the ETB near the separatrix obtained with the reference choice of parameters $\lambda_\chi = 0.20$, $\lambda_D = 0.08$ for JET discharge #79668.

In summary, our studies show that the transition from L-mode to stationary high quality H-mode in high power and high current ITER-relevant JET discharges can be reproduced well in JINTRAC-Core+SOL simulations provided that a gradual reduction of anomalous transport in the ETB takes place with increasing $P_{net}/P_{L\text{-}H}$ and with a faster reduction in particle transport compared to energy transport ($\lambda_\chi/\lambda_D > 1$). Combining this assumption regarding transport ETB with an extension of the ETB transport in the near-SOL and applying the theory based transport model GLF23 for the description of core anomalous energy and particle transport provides results that can reproduce all major features of evolution of the plasma parameters from the core to the SOL and divertor. This includes the relaxation of the main ion and carbon density profiles in this phase, the changes to the SOL and ETB density and temperature profiles and the power and particle fluxes to the divertor, although for the latter the in-out divertor asymmetry cannot be reproduced. The results are not very sensitive to the applied gas puffing rate and the precise value of pumping efficiency due the relatively low efficiency of puffed and recycled neutrals to fuel the ETB plasma in JET for these conditions, caused by SOL ionisation, which is modelled to be even lower in ITER.

The successful validation of transport models and modelling assumptions for the prediction of the behaviour of ITER-relevant plasmas in the transition to high quality H-mode in JET is an important step for the application of a similar approach with JINTRAC to the modelling of high Q_{DT} H-mode access in ITER described below.

4. Modelling of access to high Q_{DT} H-mode in ITER 15 MA DT plasmas and fuelling optimization.

Extensive transport modelling studies have been carried out in the past [Parail NF 2009, Loarte NF 2013, Parail NF 2013, Casper NF 2014, Kessel NF 2009] to determine whether stationary burning H-mode conditions can be reached in the ITER baseline scenario flat-top phase which are required to meet the primary ITER performance target of a fusion yield ratio $Q_{DT} \sim 10$ [Shimada NF 2007]. In this respect, the transition phase from low density L-mode (~20-40% of Greenwald density n_{GW}) with I_p ~15 MA to a stationary high confinement H-mode plasma at high density (>~70% of n_{GW}) with substantial fusion power production was found to be critical in the past and in more recent studies [Kessel NF 2015]. In stationary $Q_{DT} \sim 10$ H-mode conditions ITER will operate with $P_{net}/P_{L\text{-}H} \sim 2$ corresponding to $P_{sep}/P_{L\text{-}H} \sim 1.3\text{-}1.5$ and with $P_{AUX} \leq P_{L\text{-}H}$. The contribution of the alpha heating is therefore essential to maintain the ITER plasmas in stationary high Q_{DT} H-mode and also to allow the access to these high confinement conditions themselves. The level of alpha heating is strongly dependent on the values of plasma density and temperature and thus the energy confinement in the plasma; in particular $T_i > 10$ keV is required for the cross section of the DT reaction to be sizeable. Similarly the H-mode threshold power is found to depend on density as $P_{L\text{-}H} \propto n_{e,lin.}^{0.717}$ [Martin JPhys 2008] and thus a high plasma density increases the required edge power flow to sustain the plasma in the H-mode regime. As it will be shown below, access to the high Q_{DT} H-mode in ITER depends on the build-up of the alpha heating power and in maintaining a sufficient margin above the L-H threshold. Both of these are determined by the plasma density evolution in ITER, directly through the H-mode threshold or indirectly through its effect on DT reactivity and this will therefore the focus of our studies.

Contrary to present experiments, the control of the plasma density evolution following L-H transitions is expected to be much easier in ITER. This is due to the fact that gas puffing and recycling neutrals have a very low fuelling efficiency of the core plasma in ITER [Kukushkin FED 2011] so that the gas puffing level influences the value of the separatrix density but much less the density gradient in the ETB due to the low ionisation source. The density gradient in the ETB in ITER, which determines the minimum level of the core plasma density, is thus determined by the outflow of particles from the plasma core which is compensated by pellet fuelling. Pellet injection in ITER is expected to provide a peaked source with typical deposition centre at $\rho_{norm} \sim 0.85$ [Pégourié PPCF 2009]. The characteristic time for the propagation of deposited pellet particles to the core is strongly affected by the presence of an anomalous, inwards directed particle pinch that depends on the level of collisionality [Angioni PoP 2007]. In addition to the edge density gradient that can be controlled by pellet fuelling in ITER, the temperature profiles develop a gradient in the ETB following the H-mode transition in ITER. This gradient increases with the decrease of anomalous transport as the edge power flow increases above the L-H transition reaching, ultimately, the edge MHD stability limit and leading to the triggering of ELMs. In this respect, the ITER plasmas are expected to behave in a way similar to those in present experiments with respect to the build-up of the edge pressure gradient from L-mode to the stationary H-mode with the only difference that in ITER the contribution of

the edge density gradient to the edge pressure gradient build-up can be controlled by pellet fuelling during the high performance H-mode access phase.

Since ITER scenario modelling studies have mainly been performed in the past under simplified conditions for the modelling of the L-H transition (i.e. by the arbitrary prescription of an instantaneous transition from L-mode to high quality H-mode) and for particle transport (i.e. prescribed density evolution) the effects and their inter-dependencies have not been properly taken into account. In fact, the limitations of operational space in the transition from L-mode to stationary burning H-mode in ITER can only be properly evaluated by means of fully predictive integrated simulations including core and edge energy and particle transport and with experimentally validated models for the plasma behaviour in this transient phase. Optimization of this transition phase can then be performed on the basis of various criteria which can include the robustness of the transition from L-mode to high Q_{DT} H-mode to small perturbations in plasma parameters, the minimisation of resistive flux consumption to allow longer burn lengths and the avoidance of W contamination of the confined plasma. It is important to note that the two plasma conditions whose transition we study are dictated by overall requirements of the ITER scenarios, design and fusion performance objectives. Namely, we consider the transition between a low density L-mode (~20-40% of Greenwald density n_{GW}) plasma with I_p = 15 MA to a stationary high confinement H-mode plasma at high density ($\geq$ 80% of n_{GW}) with substantial fusion power production and with an additional power level $P_{AUX} \leq 73$ MW.

To study the physics phenomena that affect plasma behaviour in the phase from L-mode to high Q_{DT} H-modes in the ITER 15MA/5.3T scenario, an extensive set of fully-predictive simulations have been performed with JINTRAC-Core including the model to reduce anomalous transport in the ETB following the H-mode transition that has been validated against ITER-relevant JET discharges. The studies include the first systematic assessment of the effect of the plasma density evolution on the access to high Q_{DT} H-mode plasmas in ITER and sensitivity analysis of this access with respect to the level of additional heating, maximum pedestal pressure allowed by edge MHD stability and uncertainties in the prediction of P_{L-H} for ITER.

The simulations start at the end of current ramp-up (t = 70 s) with an ITER 15 MA / 5.3 T DT L-mode plasma corresponding to an ITER Q_{DT} = 10 baseline scenario plasma where the current ramp-up has been optimised to avoid limits in the PF coil system and to achieve sufficiently high magnetic shear to avoid core plasma confinement deterioration (see [Parail NF 2013] for further details of Case#001). Auxiliary heating of either P_{AUX} = 53 MW or P_{AUX} = 63 MW (consisting of 33 MW of NB power, 20 MW of ECRH, and, in the second case, another 10 MW of ICRH) is applied immediately after the start of the simulation leading to a fast increase in the edge power flux above the L-H transition power threshold and to triggering the transition into H-mode. The auxiliary power level is maintained at the same level for the entire simulated phase. For CPU time efficiency the extensive set of simulations reported here have been carried out with the JINTRAC-Core model instead of the JINTRAC-Core+SOL model, as the CPU requirements for the latter do not allow such a large set of simulations to be carried out. To ensure a proper inclusion of SOL plasma effects in our simulations, the values of the plasma parameters at the

separatrix and the maximum pedestal pressure compatible with edge MHD stability and the width of the ETB have been evaluated with the ITER EPED1-SOLPS scaling [Pacher JNM 2007, Polevoi NF 2015]. This is an approach that has been shown to provide similar results to those from the full JINTRAC-Core+SOL model for stationary L-mode and H-mode plasmas in ITER [Romanelli NF 2015, Polevoi NF 2016]. The neutral influx across the separatrix is also taken to be consistent with full integrated simulations of ITER plasmas [Romanelli NF 2015] and previous ITER edge plasma simulation studies which show that the maximum neutral influx across the separatrix $\Gamma_{D,neut,sep} = \Gamma_{T,neut,sep} \leq 10^{22}$/s for an edge power flow level = 50 – 150 MW [Pacher JNM 2011]. Further core particle fuelling (in addition to particle sources from neutral beams which are negligible in ITER; 33 MW of 1 MeV NBI neutrals provide a total core source of $2 \cdot 10^{20}$ s^{-1} and the neutral influx across the separatrix described above) is provided by injection of pellets, which are modelled in these scans in a time-averaged way by application of a continuous particle source that is normalised to a desired pellet particle fuelling rate determined by feedback control to achieve a prescribed density evolution. The characteristic feedback reaction time is assumed to be ~0.5 s.

The transport model and modelling assumptions applied to ITER are the same as those used for JET modelling. Anomalous core transport is described by GLF23 for H-mode plasma conditions while the BgB model is used in L-mode. The anomalous transport in the ETB is assumed to decrease following the H-mode transition with P_{net}/P_{L-H} in the same fashion as found to describe the JET experiments ($\lambda_\chi = 0.20$, $\lambda_D = 0.08$). Core impurity transport of He, Ne and W has been modelled with SANCO. Boundary conditions for the impurity ion and neutral fluxes at the separatrix have been feedback-controlled in order to maintain a minimum constant line-averaged W density of $\sim 5 \cdot 10^{13}/m^3$. This is a very low W density (W concentration $< 10^{-6}$) and corresponds to a trace impurity concentration at which the presence of W has no impact on the plasma evolution but allows the characterization of W transport and the evaluation of plasma conditions which are, or are not prone to W accumulation. The line-averaged densities of He and Ne are allowed to vary with time in order to roughly maintain a line-averaged effective charge number of $Z_{eff} \sim 1.5$, with He and Ne contributing to an increase in Z_{eff} of ~0.1 and ~0.4 respectively, which are typical values expected in ITER [Kukushkin NF 2002]. Toroidal rotation has been taken into account in the ITER simulations, considering the torque from NB heating and applying a Prandtl number of 0.75.

In these simulations the plasma density is increased from the initial value before the auxiliary heating is applied according to the waveform in Fig. 24 with feedback controlled pellet fuelling. In an initial phase the density is maintained at typical L-mode values of $\sim 3.0\text{-}4.0 \cdot 10^{19}$ m^{-3} by gas fuelling only. The application of strong plasma heating leads to a slight increase of the average plasma density with gas fuelling due to the need to increase the separatrix density at a value sufficient to provide divertor power loads under 10 MWm^{-2} (given by the EPED1-SOLPS boundary conditions) and because of the development of an anomalous inward pinch with increasing core temperature and continuously reduced collisionality. Following this gas-only fuelled phase, pellet fuelling is applied to increase the average plasma density linearly in time to a final value of 10^{20} m^{-3}, which is typical of 15MA/5.3T high Q_{DT} operation in ITER. Both the

length of the initial gas fuelled phase and the duration of the pellet fuelled density ramp have been varied and their effect on the access to high Q_{DT} H-mode plasmas in ITER assessed. Fig. 25 summarises the results obtained for an additional power level of 53 MW. Discharges for which either the gas fuelled phase is too short or the density ramp by pellet fuelling is too fast fail to achieve high Q_{DT} H-mode plasmas and either stay in a degraded H-mode confinement or return to L-mode.

The reason for this is illustrated in Fig. 26 where two similar discharges with a pellet fuelled density ramp of 15 s and 20s are shown. A too fast increase of the plasma density following the start of the high heating phase leads to a decrease of the plasma temperature and, consequently, of the alpha heating power. In this respect, it is critical that for a sufficient volume of core plasma the ion temperature remains higher than 10 keV during the pellet fuelled density ramp phase – otherwise the fusion power decreases at constant ion core pressure as the density in the core is increased, whereas it only depends on the ion pressure at temperatures of 10 keV and higher for which the scaling $P_{fus} \propto \sim (n_i T_i)^2$ is valid. The decrease of the fusion power for fast pellet fuelled density ramps together with the increase of the H-mode threshold power with plasma density leads to an insufficient $P_{net}/P_{L\text{-}H}$ level to decrease anomalous transport in the pedestal which leads to the plasma staying in a low quality H-mode with low pedestal pressure and Q_{DT} and a final return to L-mode conditions as the density is increased further, illustrated in Fig. 26 for the faster pellet fuelled ramp case.

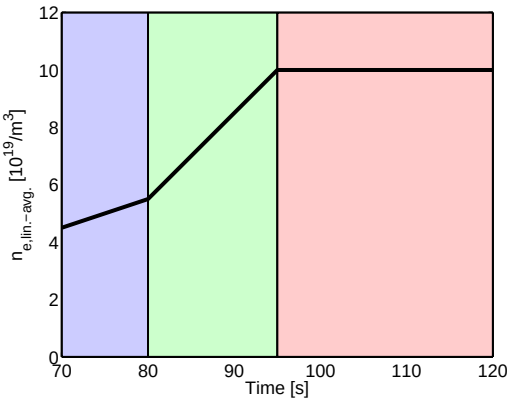

Figure 24: Template waveform of the average plasma density considered in our studies indicating the gas fuelled-only phase (blue-shaded) and the pellet fuelled density ramp (green-shaded) and high density (red-shaded) phases.

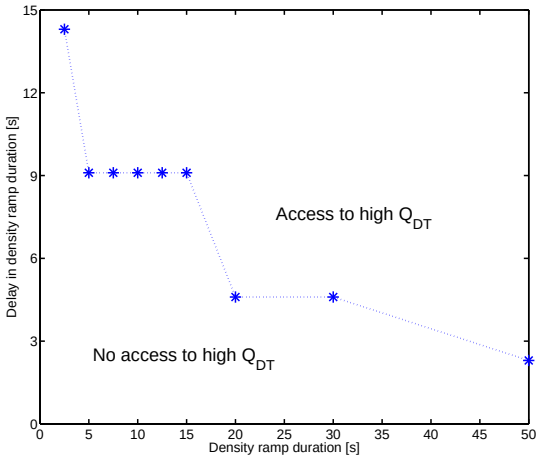

Figure 25: Operational space for the achievement of a transition to high Q_{DT} ~ 10 15MA/5.3T H-mode in ITER for P_{AUX} = 53 MW in terms of the duration of the pellet fuelled ramp to the nominal density and of the delay of the ramp in density with respect to the start of the high heating power.

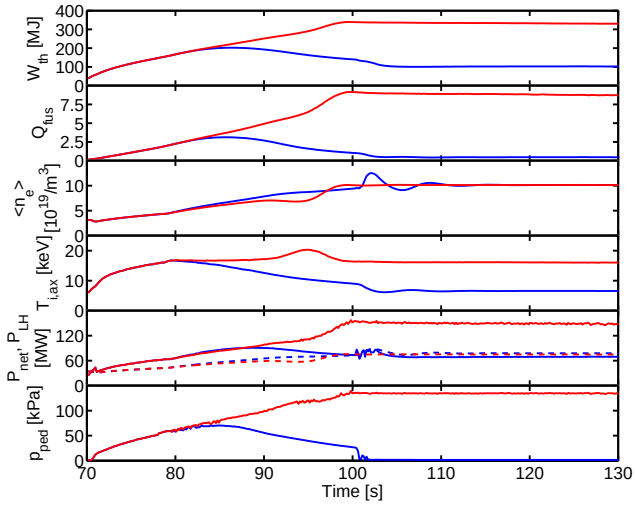

Figure 26: From top to bottom: plasma energy (W_{th}), fusion power amplification factor (Q_{DT}), plasma average density $<n_e>$, ion temperature on axis ($T_{i,ax}$), P_{net} (solid) and P_{L-H} (dashed), and pedestal pressure (p_{ped}) for a successful (red) and unsuccessful (blue) transition to high Q_{DT} H-mode with P_{AUX} = 53 MW for two pellet fuelled density ramp durations of 20 s (red) vs. 15 s (blue).

Analysis of the results in Fig. 25 shows that the physics parameter that influences the access to stationary H-mode at high Q_{DT} in ITER is not the length of the gas fuelled phase as such but the value of Q_{DT} that has been achieved at the start of the pellet-fuelled density ramp. The length of the gas fuelled phase is thus important because in this phase the Q_{DT} and alpha heating power produced by the plasma increase in time as the plasma temperature increases to values T_i > 10

keV over a significant fraction of the plasma volume following the H-mode transition. This allows the reformulation of Fig. 25 in terms of Q_{DT} at the beginning of the pellet fuelled density ramp and of its duration as shown in Fig. 27.

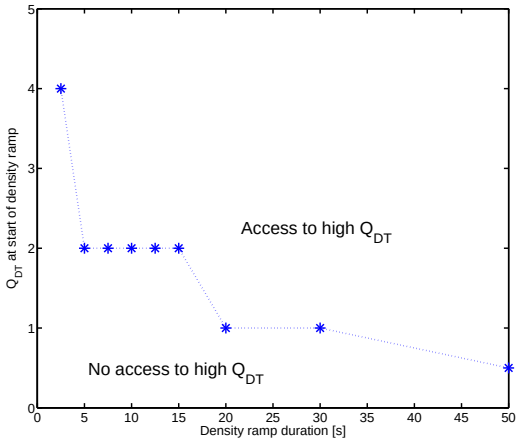

Figure 27: Operational space for the achievement of a transition to high Q_{DT} 15MA/5.3T H-mode in ITER for P_{AUX} = 53 MW in terms of the value of Q_{DT} at the beginning of the duration of the pellet fuelled density ramp to the nominal density.

In this respect, it is interesting to note that increasing the level of additional heating during the L-mode to stationary H-mode phase has a significant effect on the operational space for the achievement of high Q_{DT}. At the level of P_{AUX} = 63 MW this space is significantly broadened as shown in Fig. 28, with only very fast density ramps (< 5 s) or plasmas with very low Q_{DT} before the ramp (< 0.5-1.0) failing to achieve the transition.

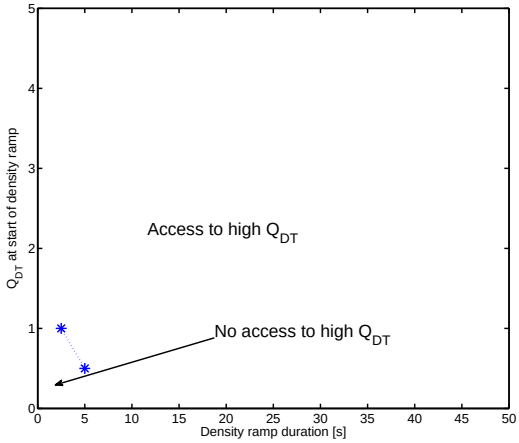

Figure 28: Operational space for the achievement of a transition to high Q_{DT} 15MA/5.3T H-mode in ITER for P_{AUX} = 63 MW in terms of the value of Q_{DT} at the beginning of the duration of the pellet fuelled density ramp to the nominal density.

This is shown in more detail in Fig. 29 where the access to high Q_{DT} H-mode in ITER is modelled for a range of P_{AUX} = 53-73 MW for simulations discharges with the same Q_{DT} ~ 2.0 at the start of the pellet fuelled ramp in density with a density ramp duration of 15 s. While the transition to stationary H-mode at high Q_{DT} is successful at P_{AUX} = 73 MW and 63 MW, the plasma remains in a low confinement H-mode and finally returns to L-mode for P_{AUX} = 53 MW. As explained above, this is due to a combination of the P_{net} required to sustain a high quality H-mode and the lower T_i and fusion power production in these conditions that reduces P_{net}. It should be noted that the Q_{DT} in the stationary phase of these plasmas with P_{AUX} > 53 MW remains at Q_{DT} ~ 6. This is due to the moderate increase of plasma energy and fusion power with $P_{tot} = P_{AUX} + P_{\alpha}$ despite the more substantial increase of P_{AUX} (by 20% for 63 MW and 40% for 73 MW), which is consistent with the degradation of H-mode energy confinement with heating power in the ITER H_{98} (y,2) scaling law [ITER NF 1999].

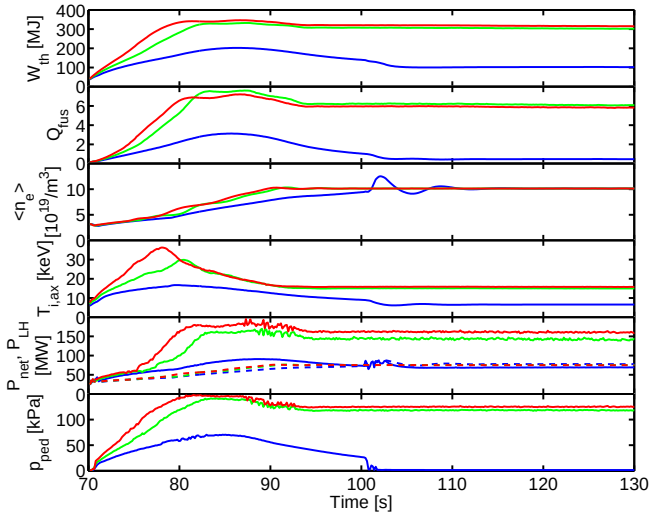

Figure 29: From top to bottom: plasma energy (W_{th}), fusion power amplification factor (Q_{DT}), plasma average density $<n_e>$, ion temperature on axis ($T_{i,ax}$), P_{net} (solid) and P_{L-H} (dashed), and pedestal pressure (p_{ped}). A successful transition to high Q_{DT} H-mode in ITER is achieved with the pellet fuelled density ramp starting at Q_{DT} ~ 2.0 and with a density ramp duration of 15 s with P_{AUX} = 73 MW (red), 63 MW (green). For P_{AUX} = 53 MW (blue) the plasma remains in a low confinement H-mode and finally returns to L-mode.

As seen in Figure 26, modelling of the core plasma anomalous transport with GLF-23 and the pedestal-SOL plasma characteristic with the EPED1-SOLPS scalings leads to a maximum plasma pressure on top of the pedestal of $p_{ped,max}$ ~ 120-130 kPa and, for a plasma density close to the Greenwald limit, to a fusion gain of Q_{DT} ~ 8 in stationary burning conditions for P_{AUX} = 53 MW, which is in agreement with previous results [Polevoi NF 2015]. To study the sensitivity of the access to stationary high Q_{DT} H-modes to the fusion performance in stationary conditions we have adjusted the maximum value of the plasma pressure on top of the pedestal in stationary

conditions to $p_{ped,max}$ ~ 150 kPa, which yields Q_{DT} ~ 10 in stationary conditions for P_{AUX} = 53 MW and repeated density ramp scans studies similar to those above for Q_{DT} ~ 10. Our analysis shows that the difference in terms of the minimum Q_{DT} at the start of the density ramp that ensures access to Q_{DT} = 10 for a given pellet fuelled density ramp duration is very small as shown in Fig. 30. Similarly the probability for a back transition to L-mode in the later phase of the H-mode evolution transition when pedestal pressure reaches $p_{ped,max}$ and the plasma enters the Type I ELMy H-mode is only weakly affected by the exact value of Q_{DT} and the alpha heating, which is 25% higher for Q_{DT} = 10 than for Q_{DT} = 8. By that time P_{net} is sufficiently well above P_{L-H} to ensure good H-mode confinement already for plasmas which reach stationary Q_{DT} = 8 so that this additional 25% of alpha heating power for Q_{DT} = 10 has no significant effect on broadening the space for high Q_{DT} H-mode access.

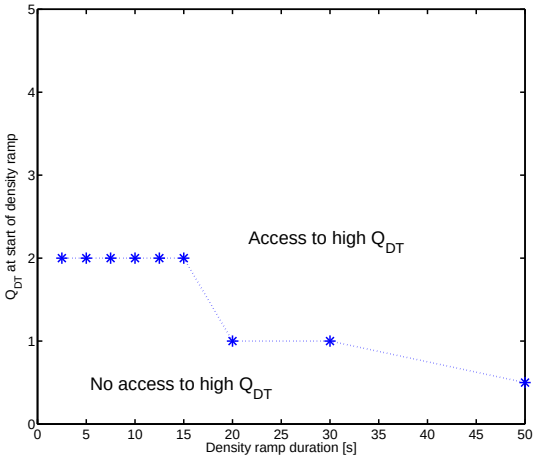

Figure 30: Operational space for the achievement of a transition to Q_{DT} = 10 15MA/5.3T H-mode in ITER for P_{AUX} = 53 MW in terms of the value of Q_{DT} at the beginning of the duration of the pellet fuelled density ramp to the nominal density.

Therefore, we have used the results of the studies for plasmas with Q_{DT} ~8 stationary fusion power gain to quantify the consumption of magnetic flux in the high Q_{DT} H-mode access phase and to determine in which way it can be minimised. This is shown in Fig. 31 where the flux consumption is plotted together with the results of Fig. 27 and 28 for the boundary in terms of Q_{DT} at the start of the density ramp and the duration of the pellet fuelled density ramp. As shown by this analysis the flux consumption in the access phase is very moderate for robust H-mode transitions with P_{AUX} = 53 MW (< 2.5 Wb). This should be compared with an inductive flux for burn of ~30 Wb in ITER and a loop voltage of ~50-75 mV for stationary high Q_{DT} H-mode expected; i.e. the resistive loss in the high Q_{DT} H-mode access phase is equivalent to < 30-50 s of burn and thus less than 10% of the ITER burn length. In addition, the resistive flux consumption in the high Q_{DT} H-mode access phase can be reduced by at least a factor of 2 by either increasing the value of Q_{DT} at the start of the pellet fuelled density ramp or by applying P_{AUX} = 63 MW in this access phase. This results from two effects: with higher starting Q_{DT} or P_{AUX} the transition takes place in a shorter time and higher plasma temperature yields lower plasma resistivity and

reduced resistive flux losses. In this respect, it appears that the same strategy that provides robust H-mode access (i.e. sufficiently long gas fuelled phase and high Q_{DT} at the start of the gas fuelled density ramp) can be combined with a moderately fast pellet fuelled ramp of 10-15 s to achieved minimum flux consumption loss in the high Q_{DT} H-mode access phase for P_{AUX} = 53 MW.

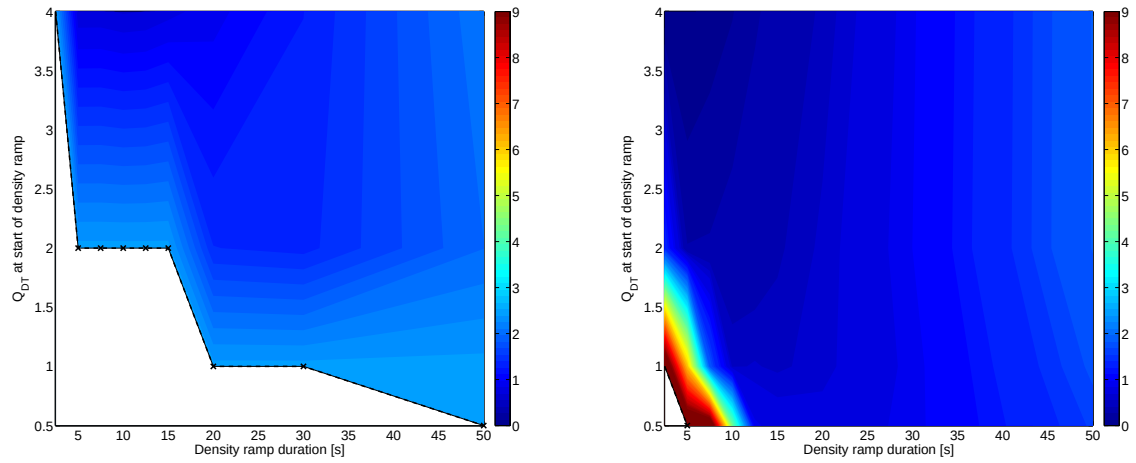

Figure 31: Contour plots for the resistive + sawtooth-induced flux consumption (in Wb) during the transition from L-mode to stationary H-mode at high Q_{DT} ~ 8 for a given density ramp duration and Q_{DT} at the start of the density ramp at P_{AUX} = 53 MW (left) and P_{AUX} = 63 MW (right). Limits for the achievement of a transition to stationary high Q_{DT} H-mode are indicated by black stars.

Inside a narrow band adjacent to the limit in density ramp conditions to achieve high Q_{DT} H-mode, the total duration until stationary H-mode at high Q_{DT} is obtained increases significantly and can even exceed the total duration of the ramp in density to $\langle n_e \rangle \sim 10^{20}/m^3$, as the plasma stays at the verge of back transition to L-mode in degraded confinement conditions with low temperature and relatively high core resistivity for a long while, and for that reason, resistive and sawtooth-induced poloidal flux consumption are considerably enhanced. The width of the band in terms of Q_{DT} at the start of the density ramp and the density ramp duration where the transition is marginal and flux consumption is enhanced, increases in size with increasing power, as the probability to maintain degraded H-mode conditions for an extended period at a low level of alpha heating with P_{net} only slightly exceeding P_{L-H} increases for higher P_{AUX}.

Because the limits in terms of pellet fuelling density ramp duration depend on P_{net}/P_{LH} and the fusion reactivity of the plasma (i.e. Q_{DT} and T_i > 10 keV over a significant plasma volume), the conditions of the L-mode plasma, before a high level of P_{AUX} is applied leading to the H-mode transition, influence these limits. For instance, maintaining a lower plasma density and significant plasma heating before the H-mode is accessed allows a higher P_{net}/P_{L-H} ratio in the initial H-mode phase (both because P_{L-H} is low and because T_i and Q_{DT} are higher) and then allows a faster ramp of the density during the pellet fuelled case. In this respect, it should be noted that the initial density considered in our studies is ~ 3.0-4.0 $10^{19}m^{-3}$ and thus already close to the minimum value ($2.6 \cdot 10^{19}/m^3$) required for unrestricted application of NBI heating with acceptable shine-

through loads and for the L-H threshold scaling applied in these studies to be valid [Ryter NF 2014] and thus there might not be much room for a reduction of the transition time compared to the results presented here by further decreasing the plasma density in the L-mode phase. On the other hand, increasing the level of alpha heating power P_α in the L-mode phase, which amounts to few MW, could in principle have an effect on the operational space for high Q_{DT} H-mode access, particularly for P_{AUX} = 53 MW. In a dedicated study it was found that as a rule of thumb, the same limits for the duration of the pellet fuelled density ramp for a given level of P_{AUX-1} in the H-mode phase can be maintained with a lower P_{AUX-2} in the H-mode phase if the initial level of P_α in the L-mode phase can be increased by $\Delta P_{AUX} = C \cdot (P_{AUX-1} - P_{AUX-2})$ via higher heating in the L-mode phase considering a multiplier C that gradually increases from ~1.0 to larger values with increasing foreseen time between the start of the ramp in density and the time of the L-H transition. Fig. 32 shows an example of this rule of thumb finding by comparing cases with P_{AUX} = 53 MW (failed transition) and 55 MW (successful transition) and negligible pre-heating in the L-mode phase with a case with P_{AUX} = 53 MW in the H-mode phase with moderate pre-heating in the L-mode phase of P_α ~2.0 MW that allows a successful transition where, without pre-heating, it was not possible. In practice, the benefit of pre-heating is limited because it is difficult to achieve a level of alpha heating larger than a few MW in L-mode as the density needs to be maintained at a low level of ~ $3.0\text{-}4.0 \cdot 10^{19} m^{-3}$ in order to minimise P_{L-H} in the early phase of the transition to H-mode and the additional heating level must be lower than this threshold value in the L-mode phase. In addition, the diffusion of edge current towards the core during and after the end of current ramp-up can be slowed down if a significant pre-heating power is applied in the L-mode phase. This makes the current density in the early H-mode phase to be less peaked than when no pre-heating is applied. The associated flatter shear profile in the pre-heating case can cause a degradation in confinement for the GLF23 core transport model used in these simulations (cf. [Parail NF 2013]) during this initial H-mode phase. This lower confinement in the initial H-mode phase when pre-heating is applied can counteract the abovementioned beneficial effects of a higher total plasma heating power in the H-mode access phase due to pre-heating.

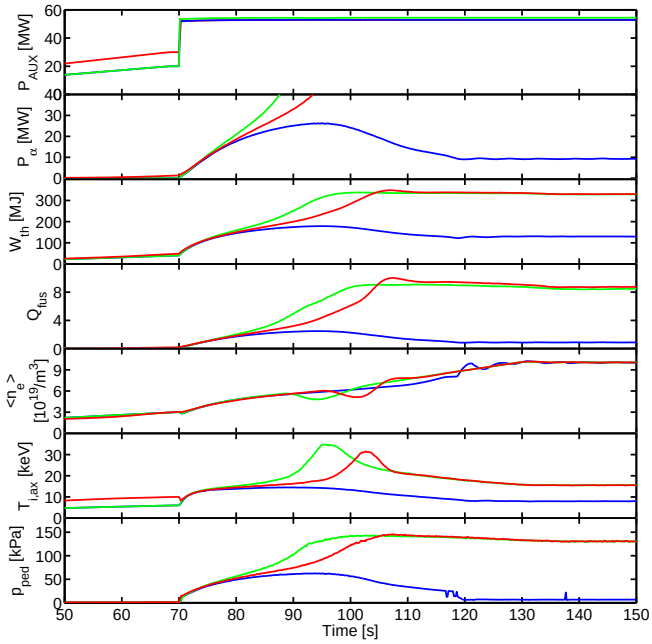

Figure 32: From top to bottom: auxiliary power (P_{AUX}) alpha power (P_{α}), plasma energy (W_{th}), fusion power amplification factor (Q_{DT}), plasma average density $<n_e>$, ion temperature on axis ($T_{i,ax}$) and pedestal pressure (p_{ped}). The current ramp-up and pre-heating phase ends at t = 70 s. The L-H transition is triggered by application of increased auxiliary heating at t ~ 70-71 s. A successful transition to high Q_{DT} H-mode in ITER is achieved with the pellet fuelled density ramp started only a few seconds later and a density ramp duration of ~50 s with P_{AUX} = 53 MW and optimised pre-heating with P_{α} ~ 2.0 MW (red) as well as with P_{AUX} ~ 55 MW with low pre-heating of P_{α} < 0.4 MW (green). For P_{AUX} = 53 MW with the same low level of pre-heating of P_{α} < 0.4 MW (blue) the plasma remains in a low confinement H-mode and finally returns to L-mode.

It is also important to note that the duration of the phase required for the achievement of high Q_{DT} H-modes ($\tau_{high\text{-}H}$) in ITER typically exceeds by a significant factor (3-10) the typical H-mode confinement time in the stationary phase $\tau_{H\text{-}mode}$ (~3.5 s in ITER). This results from the gradual reduction of the ETB anomalous transport with $P_{net}/P_{L\text{-}H}$, already identified in JET experiments, but the overall ratio of $\tau_{high\text{-}H}/\tau_{H\text{-}mode}$ in ITER ($\tau_{high\text{-}H}/\tau_{H\text{-}mode}$ ~ 3-10) is substantially larger than in the JET experiments modelled in section 2 ($\tau_{high\text{-}H}/\tau_{H\text{-}mode}$ ~ 2-3). This is due to the relatively low $P_{net}/P_{L\text{-}H}$ ratio of the ITER plasmas in the initial H-mode phases when P_{net} is dominated by the auxiliary heating (P_{net} < ~53 MW) and to the fact that, unlike in present experiments, the total plasma heating power builds up with the alpha heating power, which leads to the increase of $P_{net}/P_{L\text{-}H}$ and to the reduction of ETB anomalous transport.

The quantitative aspects of the results in this study do obviously depend on modelling assumptions. For instance, it has been observed that in JET experiments with ITER-like PFCs (W/Be) the H-mode threshold can be significantly lower (by 30-40%) than that observed for

carbon PFCs [Maggi NF 2014]. The scaling law used for the H-mode threshold power evaluation [Martin JPhys 2008] in our studies for JET and ITER was derived on data dominated by experiments with carbon PFCs and thus it does not take into account this fact. For instance, a reduction of the H-mode threshold power by 25% in ITER with respect to our assumptions would make the operational space for successful high Q_{DT} H-mode access for P_{AUX} = 53 MW to be very similar to that that we have obtained P_{AUX} = 63 MW and our standard H-mode threshold power assumptions. This is because what determines the ETB anomalous transport reduction in the H-mode transient phase is P_{net}/P_{L-H} and P_{net}/P_{L-H} with P_{AUX} = 63 MW has a similar value to $P_{net}/(0.75 \times P_{L-H})$ with P_{AUX} = 53 MW.

5. W control during L-H transition

It is known from present day experiments (including experiments on AUG and JET) that the L-H transition is usually accompanied by a rise of W sputtering at the divertor target plates due to the higher divertor temperatures. This increase in the W source can lead to an increase of the SOL W density and finally to an increase of the core W density if transport through the ETB does not prevent it. Such W density increase can then lead to higher plasma radiation in the high Q_{DT} H-mode access phase and thus to a reduced edge power flow and the return of the plasma to L-mode. The full integrated plasma simulations including both core and SOL and transport of W for plasmas at the ITER scale are extremely demanding computationally and are beyond the scope of this paper.

In our study we have therefore concentrated on two specific aspects of 1) analysing W impurity control in the high Q_{DT} H-mode access phase of ITER 15 MA scenarios and 2) investigating whether the schemes developed in section 4 to provide robust access to high Q_{DT} H-mode are compatible with the needs for W density control in the core plasma or not. In particular, we have performed JINTRAC-core and JINTRAC-core+SOL simulations for the high Q_{DT} H-mode access phase of the 15 MA ITER baseline scenario to determine what are the advantages and disadvantages with respect to W production and transport in the ETB of having an initial gas fuelled phase at moderate plasma density in H-mode then followed by a pellet fuelled phase to high Q_{DT}, as required for robust H-mode access with P_{AUX} = 53 MW.

Regarding W production in the access phase to high Q_{DT} H-mode, this is directly linked to maintaining a low divertor temperature and low sputtering yield in this phase. Regarding transport in the ETB, this is linked to the characteristics of neoclassical W transport in this region. Previous studies for ITER [Dux PPCF 2014] have revealed that W screening due to the large temperature gradients in the ITER ETB compared to the respective density gradients provides a very effective shielding of the plasma core from W being produced at the divertor for stationary high confinement H-modes in ITER. In these conditions the W density at the pedestal top can be significantly smaller (more than one order of magnitude) than that at the separatrix. We have therefore evaluated if these favourable features of the neoclassical transport for stationary high confinement H-modes in ITER are also at work for the plasma conditions in the transient phase, which are required to provide robust access to high Q_{DT} H-modes in ITER.

5.1. Simulations of W production by H-mode onset with JINTRAC-core+SOL

To study the production of W during the access phase to high Q_{DT} H-mode in ITER, full integrated JINTRAC-core+SOL simulations including Be and W transport have been carried out for the early phase of the L-H transition. Due to computational requirements, these simulations are limited in the time interval simulated. In these simulations, the transition to H-mode starts at t = 79.5 s after the auxiliary heating is increased to P_{AUX} = 53 MW. The average core density is kept at a level of 4-5·10^{19} m^{-3} by pellet fuelling without gas puffing to allow for a fast increase in core temperatures and fusion reaction rate, allowing the comparison of the effects on edge density and W behaviour to be studied when gas puffing is applied. After few seconds, pellet fuelling is removed and when quasi-stationary plasma conditions are achieved (after t = 82.8 s), three different levels of gas fuelling are applied: $\Gamma_{puff} \sim 0\ s^{-1}$, $\Gamma_{puff} \sim 10^{22}\ s^{-1}$ and $\Gamma_{puff} \sim 2\cdot10^{22}\ s^{-1}$ (similar to the gas fuelling scan in [Romanelli NF 2015]).

The results of the simulations are shown in Fig. 33. The most significant effect of gas fuelling is observed on the plasma temperature at the target plates (T_e) and on the corresponding level of W sputtering. Without gas fuelling in the H-mode access phase, T_e at the target can reach ~200 eV. This high temperature creates a strong negative electric potential near the divertor target and accelerates ions (both main ions and impurities). Hitting the target plate, these ions cause a strong sputtering of W with the effective sputtering yield reaching a level of $Y > 1\cdot10^{-2}$ (note that prompt W redeposition on the target has not been considered in these simulations). This results in a fast rise of the W content in the SOL. Applying a moderate level of gas puffing in the H-mode access phase of $\Gamma_{puff} > \sim10^{22}\ s^{-1}$ can keep the divertor plasma temperature below ~10 eV in this phase and W sputtering at negligible levels in the simulations. In addition to the effect on W sputtering, the resulting higher separatrix density affects W transport through the ETB as it will be described in more detail in the next section. The higher separatrix densities at higher fuelling rates decrease or even reverse the direction of the neo-classical W inwards pinch velocity in the ETB decreasing core plasma W contamination in the high Q_{DT} H-mode access phase. It is important to note that the reversal of the ETB W pinch from inwards to outwards-directed occurs at a higher rate of gas fuelling than that needed to avoid strong W sputtering.

These results show that accessing the H-mode in a phase with gas fuelling only, as required for robust high Q_{DT} H-mode access, is advantageous from the point of view of reducing the W source in this access phase, since the increased SOL density that can be achieved compared to pellet fuelling in this phase (due to the low fuelling efficiency of the recycling neutrals in ITER) leads to a large reduction of the divertor temperature and thus of the W sputtering yield in this phase. In addition, the low n_{ped}/n_{sep} ratios that gas fuelling provides in this phase is favourable to screen the core plasma from any residual W that may be produced in this phase; this is discussed in more detail in the next section [Polevoi NF 2015]. Note that in the time interval modelled in our simulations, gas fuelling alone is appropriate to reduce the divertor temperature. This may be insufficient for later phases of the gas fuelled H-mode case as Q_{DT} increases and dW_{th}/dt decreases and additional injection of extrinsic impurities to increase divertor radiation and to

decrease the divertor temperature will be needed. These aspects require significant computing resources and are the subject of future studies.

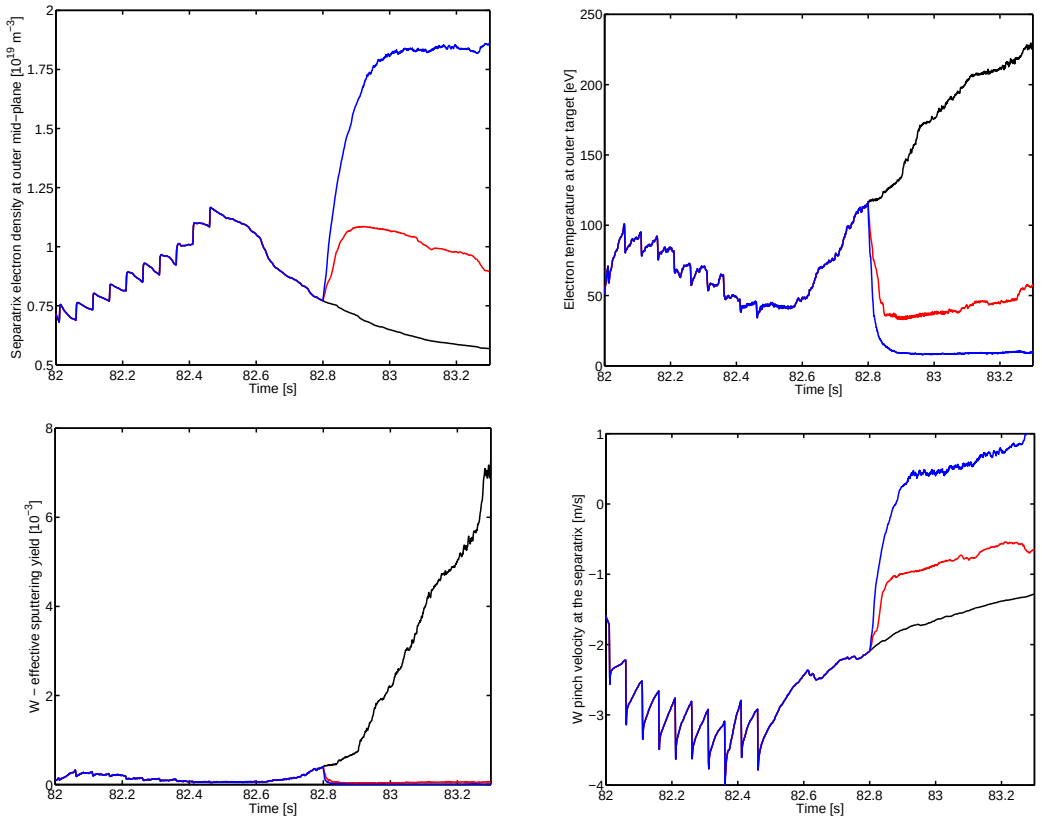

Figure 33: DT gas puff scan with JINTRAC-Core+SOL for the early H-mode phase after a L-H transition at low density in the 15 MA / 5. 3 T DT ITER baseline scenario. Left: n_e at the separatrix (outer mid-plane) (top), effective W sputtering yield (bottom). Right: T_e at the outer divertor strike point (top), W impurity pinch velocity at the separatrix (bottom), for three integrated JINTRAC-core+SOL simulations with the DT gas puff injection rate varied between $\Gamma_{puff} = 0 \cdot 10^{22}$ s^{-1} (black), $\Gamma_{puff} = 1 \cdot 10^{22}$ s^{-1} (red) and $\Gamma_{puff} = 2 \cdot 10^{22}$ s^{-1} (blue) for t > 82.8 s.

5.2. Simulations of W transport in the plasma core and ETB with JINTRAC-Core in the access phase to high Q_{DT} H-mode in ITER.

The transport in the confined plasma (including the plasma core and ETB) has been analysed for simulations that provide access to high Q_{DT} H-mode conditions in ITER with JINTRAC-Core. In these simulations a trace amount of W is assumed to be present due to a low influx of W at the separatrix to allow evaluating changes to W transport in the ETB and core plasma in the access phase to high Q_{DT} H-modes in ITER. This small W amount does not affect plasma radiation as the goal of our studies is to compare in a relative sense the advantages or disadvantages of various choices to access high Q_{DT} H-modes in ITER with respect to W accumulation, not to

evaluate core plasma W density in an absolute sense. The latter would require fully integrated JINTRAC-Core+SOL simulations of the type presented in the previous section but extended over many tens of seconds, which are beyond the scope of this paper.

In general, it is found that the good W screening in the ETB by neoclassical transport, originally identified for stationary high energy confinement H-modes, takes place during the H-mode access phase also. The physics mechanisms at work are the same. Namely, the build-up of a significant temperature gradient following the H-mode transition occurs on time scales faster than for the density, as the neutral ionisation source inside the separatrix in ITER is very small, and this leads to an outwards pinch velocity for W in the pedestal [Dux FEC 2014]. In this respect, access to high Q_{DT} H-mode with long gas fuelled phases and long pellet fuelled density ramps are optimum to maximize W screening in the ETB, as shown in Fig. 34. In this figure the overall evolution of plasma parameters in the access phase is shown for a simulation with P_{AUX} = 53 MW and a gas fuelled H-mode phase of 15 s and a pellet fuelled density ramp of 50 s together with the plasma density and temperature profiles at several times and the corresponding normalized (to $n_{sep,W}$) W density and neoclassical pinch profiles in the confined plasma. The fuelling choices (long gas fuelled phase and slow pellet fuelled density ramp) for the access to high Q_{DT} H-mode are indeed excellent to provide very good screening of the core plasma from the W density in the SOL. These conditions are also the best to provide a robust access to high Q_{DT} H-modes in ITER, as shown in section 4, but they are not optimum to minimise resistive flux consumption in this phase.

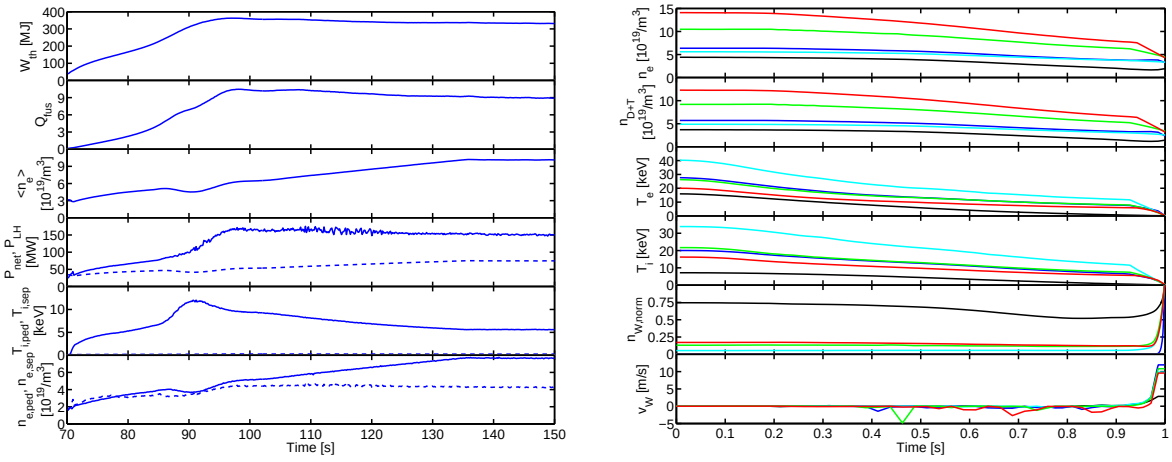

Figure 34: Transition to high Q_{DT} H-mode with P_{AUX} = 53 MW for a pellet fuelled density ramp duration of ~50 s after a gas-fuelled H-mode phase of ~15 s. Left, from top to bottom: plasma energy (W_{th}), fusion power amplification factor (Q_{DT}), plasma average density $<n_e>$, P_{net} (solid) and P_{L-H} (dashed), ion temperature on top of the pedestal (solid, $T_{i,ped}$) and at the separatrix (dashed, $T_{i,sep}$), density on top of the pedestal (solid, $n_{e,ped}$) and at the separatrix (dashed, $n_{e,sep}$). Right, from top to bottom: plasma profiles of electron density (n_e), main ion density (n_{D+T}), electron temperature (T_e), ion temperature (T_i), W density normalised to n_W at the separatrix ($n_W/n_{W,sep}$), total W convective velocity (v_W) for t = 70 s (black, L-mode

phase), ~84 s (blue, end of gas-fuelled H-mode phase), 90 s (cyan, early density ramp phase). 115 s (green, late density ramp phase), 150 s (red, stationary burn at high density).

A reduction of the resistive flux consumption requires a faster pellet-fuelled density ramp and this is potentially worse for core W accumulation in the access phase to high Q_{DT} H-mode as the temperature gradients in the pedestal would be decreased and the density gradients increased thus reducing the temperature screening in the pedestal. To evaluate whether this can lead to increased W densities in the core plasma, two simulations have been compared for the fastest pellet-fuelled density ramps that allow successful transition to high Q_{DT} H-mode in ITER with P_{AUX} = 53 MW with values of Q_{DT} = 1 and 4 at the beginning of the density ramp. The W influx across the separatrix has been kept fixed in these simulations at $\Gamma_{W,sep,in} = 2 \cdot 10^{17}$/s. Results for the overall evolution of plasma parameters in the access phase are shown together with the plasma density and temperature profiles at several times and the corresponding normalized W density and neoclassical pinch profiles in the confined plasma for both simulations (see Figs. 35-36). Although in both cases temperature screening dominates W transport in the ETB with outwards pinch velocities in the pedestal, the slower pellet fuelled density ramp required for the case with Q_{DT} = 1 provides lower core W contamination (lower $n_{ax,W}/n_{sep,W}$) than the faster pellet fuelled ramp that is possible with a starting Q_{DT} = 4. The slower density ramp leads to a much lower density at the pedestal top for the case Q_{DT} = 1 as the pedestal temperature builds up while the densities required at the separatrix to maintain the divertor power flux under 10 MWm^{-2} (evaluated with the ITER-EPED1-SOLPS scaling) are similar. The separatrix density in this scaling depends on the edge power flow as $n_{sep} \propto P_{sep}^{0.55}$. For an initial edge power flow ratio 50% higher for Q_{DT} = 4 than for Q_{DT} = 1 this leads to a 25% higher separatrix density for Q_{DT} = 4 but the much faster increase of the pedestal density by pellet fuelling leads to a larger density gradient and a weaker outwards W neoclassical pinch, particularly towards the end of the density ramp.

This analysis shows that good screening of W in the pedestal is maintained in all cases that access the high Q_{DT} H-mode in ITER and that, therefore, the plasma fuelling schemes providing robust access to high Q_{DT} H-mode in ITER are also suitable to provide low contamination of the core plasma by W during this phase. However, minimising resistive flux consumption in the access phase to high Q_{DT} H-mode in ITER by decreasing the duration of the pellet-fuelled density ramp has a negative impact on the reduction of the core W density during this phase. To determine, which fuelling strategy provides the optimum solution to resistive flux consumption and W contamination in the access phase to high Q_{DT} H-mode in ITER, the quantitative determination of the W source is required. Therefore, full integrated JINTRAC-Core+SOL simulations will be carried out in the future.

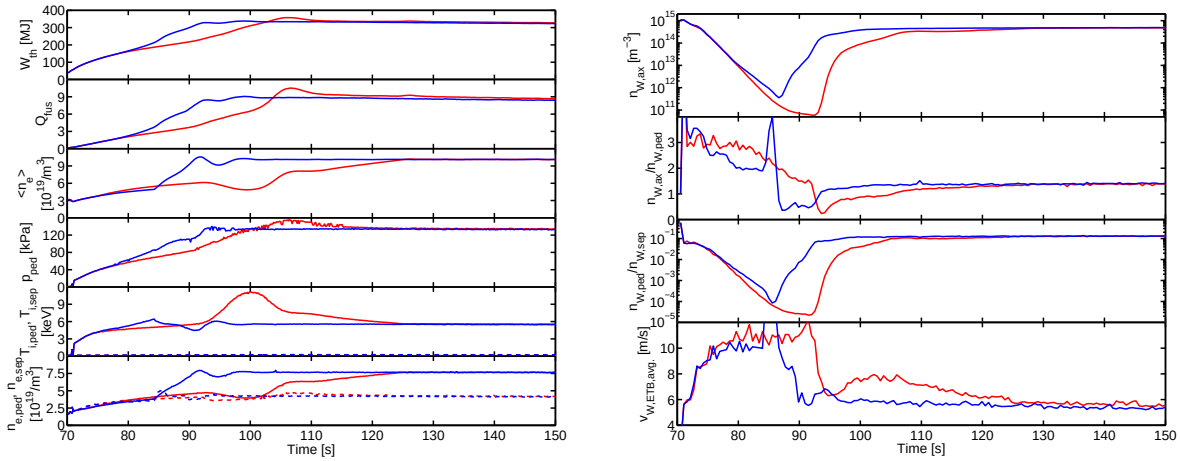

Figure 35: Left: P_{sep}, Q_{DT}, $\langle n_e \rangle$, p_{ped}, $T_{i,ped}$ (solid) and $T_{i,sep}$ (dashed), $n_{e,ped}$ (solid) and $n_{e,sep}$ (dashed), right: $n_{W,ax}$, $n_{W,ax}/n_{W,ped}$, $n_{W,ped}/n_{W,sep}$ and averaged W convective velocity within ETB, for simulation cases with the minimum density ramp duration for which a successful transition to stationary high Q_{DT} H-mode can be achieved with the density ramp starting at $Q_{DT} \sim 1.0$ (red) and $Q_{DT} \sim 4.0$ (blue).

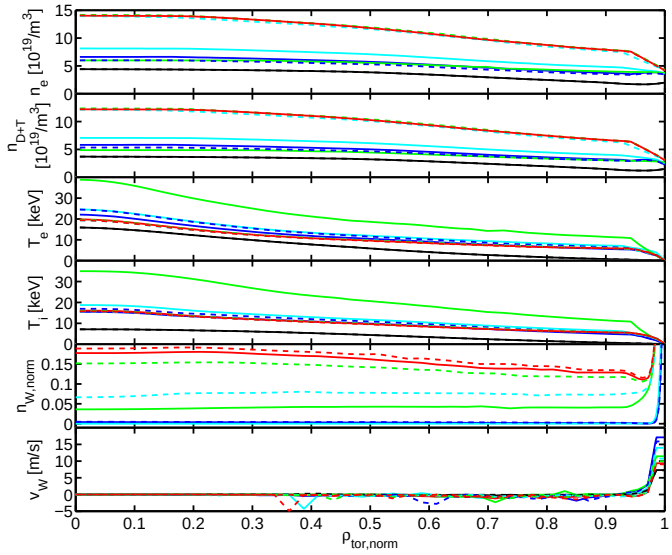

Figure 36: From top to bottom: Profiles of n_e, n_{D+T}, T_e, T_i, $n_W/n_{W,sep}$ and v_W at t ~ 70 s (black), 80 s (blue), 93 s (cyan), 100 s (green) and 150 s (red), for simulation cases with the minimum density ramp duration for which a successful transition to stationary high Q_{DT} H-mode can be achieved with the density ramp starting at $Q_{DT} \sim 1.0$ (solid) and $Q_{DT} \sim 4.0$ (dashed).

6. Summary and conclusions

Limits for the length of the gas fuelled H-mode phase and the follow-up pellet fuelled density ramp rate from L-mode densities to the densities required for high Q_{DT} in ITER with respect to the increase of auxiliary heating for the transition from L-mode to high Q_{DT} 15 MA H-mode plasmas in ITER have been established by modelling with the JINTRAC integrated modelling suite. A sufficiently long gas fuelled phase and/or a low density ramp rate are found to be required to ensure a reliable access to high Q_{DT} in ITER with P_{AUX} = 53 MW. Exceeding these limits leads to the plasma to remain in poor quality H-mode for extended periods of time or to return to L-mode confinement, in these cases $P_{net} \sim P_{L\text{-}H}$, during most of the phase after the L-H transition and the pedestal pressure remains under the Type I ELMy H-mode edge MHD stability limit.

The exact values of the gas-fuelled phase and of the pellet-fuelled density ramp depend on modelling assumptions such as the core transport model, the required power to access the H-mode and on the reduction of anomalous transport in the ETB as the power flow exceeds the H-mode threshold power. JET high current discharges with ITER-like H-modes (in the sense of low collisionality and edge density behaviour) have been modelled to validate the modelling assumptions applied to ITER. This exercise has shown that:

- the core transport model GLF23 is appropriate to describe the evolution of the core plasma parameters in the phase after the H-mode transition to stationary H-mode conditions in JET, including the relaxation of hollow density profiles observed in this phase.
- the reduction of the energy and particle anomalous transport in the ETB and the near-SOL, as the edge power flow exceeds the H-mode threshold power, is stronger for particle transport than for energy transport.

With these assumptions it has been possible to reproduce in a fully integrated and self-consistent way, for the first time, the evolution of the measured core, pedestal and SOL plasma parameters as well as the particle and power fluxes to the divertor targets in the transition from L-mode to stationary high confinement H-mode within the limitations of the model (the outer divertor is well reproduced but not the inner divertor due to lack of drifts in the edge modelling). In this respect the faster reduction of the edge particle transport compared to the thermal transport as the edge power exceeds the H-mode threshold power is essential to describe the differences between edge density and edge temperature evolution because the particle source in the core plasma by gas-fuelled and recycled neutrals is not increased after the H-mode transition, due to increased SOL ionisation in this phase.

On the basis of these assumptions, the optimization of the access to high Q_{DT} H-mode conditions in ITER to ensure robustness in the H-mode access and to reduce the loss of resistive flux during this phase (to less than 10% of the flux available for the whole burn in ITER) has been analysed. This optimization is possible by :

- adjusting the duration of the gas fuelled H-mode phase and the follow-up pellet fuelled density ramp duration to high Q_{DT} H-mode.

- increasing the level of additional heating in the high Q_{DT} H-mode phase $P_{AUX} \geq 63$ MW.
- increasing the level of additional heating in the gas fuelled L-mode phase before the high P_{AUX} phase.

These studies have also demonstrated that this operational scheme of establishing a gas fuelled H-mode phase before increasing the plasma density by pellet fuelling to high Q_{DT} H-modes in ITER is not only required for robust H-mode access but it is also advantageous to minimise contamination of the core plasma by W during this phase. This results from the use of gas fuelling during the initial phase that favours low divertor temperatures and low W production by sputtering at the divertor and the favourable neoclassical transport in the ITER pedestal during this phase. The low pedestal densities associated with gas fuelling and the slow pellet fuelled density ramp lead to the pedestal temperature to reach values $T > 5$ keV in this phase and thus to temperature screening to dominate W transport and to a strong outwards pinch for the W ions in the pedestal in the high Q_{DT} H-mode access phase which minimises core contamination. Our studies show that, although good W screening of the core plasma is achieved for all conditions which access robustly the high Q_{DT} H-mode in ITER, there is a balance between minimising core plasma contamination by W and minimising resistive flux consumption in this phase. The conditions which ensure robust H-mode access and lowest W contamination of the core plasma are those with the highest resistive consumption (although still less than 10% of the flux available for the whole burn in ITER) and vice-versa.

In conclusion our studies have demonstrated that by means of integrated JINTRAC modelling validated against transitions to high performance H-mode at JET, it is possible to optimise the evolution of plasma density by applying the ITER fuelling schemes (gas fuelling and pellets) to robustly access the high Q_{DT} H-mode scenarios required to demonstrate the ITER $Q_{DT} = 10$ goal with additional heating levels of $P_{AUX} \geq 53$ MW. In addition, the fuelling strategies that ensure robust access to high Q_{DT} H-mode plasmas in ITER are also optimum for the minimisation of core plasma contamination by W produced at the divertor target. Some of the quantitative findings of our studies are dependent on specific modelling assumptions and these will be refined in the future as our understanding of the physics processes that dominate plasma transport in the core, edge transport barrier and SOL/divertor plasmas improves.

Disclaimer: ITER is the Nuclear Facility INB no. 174. The views and opinions expressed herein do not necessarily reflect those of the ITER Organization. The views and opinions expressed do not necessarily reflect those of Fusion for Energy which is not liable for any use that may be made of the information contained herein. This work has been carried out within the framework of the EUROfusion Consortium and has received funding from the Euratom research and training programme 2014-2018 under grant agreement No 633053. The views and opinions expressed herein do not necessarily reflect those of the European Commission.

References

[Angioni PoP 2007] Angioni C. et al., Phys. Plasmas 14 (2007) 055905.

[Baiocchi NF 2015] Baiocchi B. et al., Nucl. Fusion 55 (2015) 123001.

[Behringer IAEA 1981] Behringer K., Engelhardt W. and Fussman C., Proceedings of the IAEA Technical Committee Meeting on Divertors and Impurity Control (Keilhacker M., and Deybeige U. editors) Max Planck Institut für Plasmaphysik-Garching - FRG (1981), 42.

[Braginski RevPP 1965] Braginski V. I., in Leontovich M. A. (ed), Rev. of Plasma Physics, Consultants Bureau, New York, 1965.

[Casper NF 2014] Casper T. et al., Nucl. Fusion 54 (2014) 013005.

[Challis NF 1989] Challis C. D. et al., Nucl. Fusion 29 (1989) 563.

[Chankin PPCF 2015] Chankin A. V. et al., Plasma Phys. Control. Fusion 57 (2015) 095002.

[Coppi NF 1981] Coppi B. and Sharky N., Nucl. Fusion 21 (1981), 1363.

[Dux FEC 2014] Dux R. et al., Proc. 25th IAEA FEC, St. Petersburg, Russia, 2014, paper TH/P3-29.

[Dux PPCF 2014] Dux R. et al., Plasma Phys. Control. Fusion 56 (2014) 124003.

[Erba JET Report 1996] Erba M. et al., JET Report JET R(96)07 (1996).

[Eriksson NF 1993] Eriksson L.G., Hellsten T. and Willen U., Nuclear Fusion 33 (1993) 1037-1048.

[Farina FSciTec 2007] Farina D., Fusion Sci. Techn. 52 (2007) 154.

[Garzotti NF 2012] Garzotti L. et al., Nucl. Fusion 52 (2012) 013002.

[Groth JNM 2015] Groth, M. et al., J. Nuc. Mat. 463 (2015) 471.

[Hawryluk NF 2009] Hawryluk R. J. et al., Nucl. Fusion 49 (2009) 065012.

[Heikkinen PoP 1995] Heikkinen J. A. et al., Phys. Plasmas 2 (1995) 3724.

[Houlberg PoP 1997] W.A. Houlberg, K.C. Shaing, S.P. Hirshman and M.C. Zarnstorff, Phys. Plasmas 4 (1997) 3230.

[ITER NF 1999] ITER Physics Expert Group on Confinement and Transport et al., Nucl. Fusion 39 (1999) 2175.

[Kadomtsev SovJPP 1975] Kadomtsev B. B., Sov. J. Plasma Phys., Vol.1, No. 5, Sept.-Oct. 1975, 389.

[Kallenbach JNM 2005] Kallenbach, et al., J. Nuc. Mat. 337–339 (2005) 381–385.

[Kessel NF 2009] Kessel C. E. et al., Nucl. Fusion 49 (2009) 085034.

[Kessel NF 2015] Kessel C. E. et al., Nucl. Fusion 55 (2015) 063038.

[Kotov PPCF 2008] Kotov, V. et al., Plasma Phys. Control. Fusion 50 (2008) 105012.

[Kukushkin FED 2011] Kukushin, A.S., et al., Fusion Eng. Des. 86 (2011) 2865.

[Kukushkin NF 2002] Kukushkin A. S. and Pacher H. D., Plasma Phys. Control. Fusion 44 (2002) 931–943.

[Loarte NF 2013] Loarte A. et al., Nucl. Fusion 53 (2013) 083031.

[Maggi NF 2014] Maggi C. F. et al., Nucl. Fusion 54 (2014) 023007.

[Martin JPhys 2008] Martin Y. R. et al., Journal of Physics: Conference Series 123 (2008) 012033.

[Militello-Asp EPS 2013] Militello-Asp, E. et al., 2013 Proc. 40th EPS Conf. on Plasma Physics (Espoo, Finland, 1–5 July 2013) vol 37D, P2.158. http://ocs.ciemat.es/EPS2013PAP/pdf/P2.158.pdf

[Neuhauser EPS 1999] Neuhauser, J. et al., 1999 Proc. 26th EPS Conf. Contr. Fusion Plasma Phys. (Maastricht, Netherlands, 14–18 June 1999) vol 23J, P4.040, 1521-1524.

[Nunes NF 2013] Nunes I. et al., Nucl. Fusion 53 (2013) 073020.

[Pacher JNM 2007] Pacher H. D. et al.. J. Nuc. Mat. 363–365 (2007) 400–406.

[Pacher JNM 2011] Pacher H. D. et al., J. Nuc. Mat. 415 (2011) S492–S496.

[Parail NF 2009] Parail V. et al., Nucl. Fusion 49 (2009) 075030.

[Parail NF 2013] Parail V. et al., Nucl. Fusion 53 (2013) 113002.
[Pégourié NF 2007] Pégourié B. et al., Nucl. Fusion 47 (2007) 44–56.
[Pégourié PPCF 2009] Pégourié B. et al., Plasma Phys. Control. Fusion 51 (2009) 124023.
[Polevoi NF 2015] Polevoi A. R. et al., Nucl. Fusion 55 (2015) 063019.
[Polevoi NF 2016] Polevoi A. R. et al., Nucl. Fusion 57 (2017) 022014.
[Romanelli NF 2015] Romanelli M. et al., Nucl. Fusion 55 (2015) 093008.
[Romanelli PFR 2014] M. Romanelli et al., Plasma and Fusion Research 9 (2014) 3403023.
[Ryter NF 2014] Ryter F. et al., Nucl. Fusion 54 (2014) 083003.
[Sartori PPCF 2004] Sartori, Plasma Phys. Control. Fusion 46 (2004) 723.
[Shimada NF 2007] Shimada M. et al., Nucl. Fusion 47 (2007) S1–17.
[Snyder PoP 2009] Snyder P. et al., Phys. Plasmas 16 (2009) 056118.
[Summers AIP 2007] Summers, H. P. et al., AIP Conf. Proc. 901 (2007) 239.
[Waltz PoP 1997] Waltz R. E. et al., Phys. Plasmas 4 (1997) 2482.
[Willensdorfer NF 2013] Willensdorfer M et al., 2013 Nucl. Fusion 53 093020.